Final Report from the University of Washington

The Staged Prevaporizing-Premixing Injector: High Pressure Evaluation

AGTSR Subaward No. 00-01-SR087

December 2002

Prepared for:
Advanced Gas Turbines Systems Research
Clemson, South Carolina

Prepared by:
Philip C. Malte, Ryan G. Edmonds, Andrew Campbell Lee,
Igor Novosselov, and Stephen de Bruyn Kops
Energy and Environmental Combustion Laboratory
Department of Mechanical Engineering
University of Washington
Seattle, Washington 98195-2600

TABLE OF CONTENTS

page

List of Tables

List of Figures

TABLE OF CONTENTS CONTINUED

LIST OF TABLES

LIST OF FIGURES

LIST OF FIGURES CONTINUED

LIST OF FIGURES CONTINUED

The Staged Prevaporizing-Premixing Injector: High Pressure Evaluation

AGTSR Subaward No. 00-01-SR087

Summary

The staged prevaporizer-premixer (SPP) is a technology for injecting liquid fuels into lean prevaporized-prevapoized (LPP) gas turbine engine combustors. The use of two levels of air temperature permits the SPP to accomplish fuel injection while controlling the auto-ignition tendency of the liquid fuels. The fuel of primary interest is diesel fuel. The first stage of the SPP uses compressor discharge air cooled by 100-200 degrees, while the second stage uses air of the full temperature of the compressor discharge. By this method, in the first stage, vaporizing of the fuel and initial mixing with the air occur at a temperature sufficiently reduced to control the auto-ignition tendency, while in the second stage, full-temperature compressor discharge air is rapidly mixed into the injector, completing the premixing process and bring the fuel-air mixture to the desired injector outlet condition.

Formative work on the SPP was conducted by Lee (2000). The reader is also referred to Lee et al. (2001), for a summary of the SPP method and formative testing, and to Lee and Malte (2001) for a description of the SPP patent.

Integration of the SPP into gas turbine cycles has been examined by Campbell and Malte (2002) and Campbell et al. (2002). This work, based on thermodynamic cycle modeling, addressed the integration of the SPP into several types of gas turbine cycles. For integration of the SPP into state-of-the-art combined cycle combustion turbines, the use of the SPP was found to reduce the overall cycle efficiency by 1-2 percent relative – less than the reduction in overall efficiency that occurs with water injection. Further, the SPP technology, by permitting LPP combustion, reduces NOx to lower levels than possible with water injection into liquid diffusion flames.

In the present work, as reported herein, the evaluation of the SPP has been continued through testing and computational fluid dynamics (CFD) modeling. Industrial partners in this work have been the Gas Turbine Fuel System Division of the Parker Hannifin Corporation, and Solar Turbines, Inc. The period of performance has been June 2000 to December 2002. The work is divided as follows:

1. Low-pressure evaluation:

    a. Rebuilt, laboratory SPP, run at a pressure of 2 atmospheres and a residence time of 12-16 milliseconds, firing a 16 cc atmospheric-pressure jet-stirred reactor (JSR), run at a temperature of 1790 K and residence time of about 1.25 millisecond. Maximum temperatures in the SPP were 435 degrees C (first stage) and 550 degrees C (second stage). No deposits of carbon or hydrocarbon residues were found in the SPP. These tests demonstrated NOx emissions for diesel fuel of 6 ppmv (15% O_2 dry).

    b. Rebuilt, laboratory SPP, run at a pressure of 1.4 atmospheres and a residence time of 5-8 milliseconds, firing a 64 cc atmospheric-pressure jet-stirred reactor (JSR), run at a temperature of 1790 K and residence time of about 4 milliseconds. NOx level was 7-8 ppmv (15% O_2 dry). These tests demonstrated running of the SPP at the reduced residence time of less than 6 ms.

    c. Rebuilt, laboratory SPP, run at a pressure of 1 atmospheres and a residence time of 4-10 milliseconds, with the outlet stream of the SPP examined by laser Rayleigh scattering (LRS). The scattering test volume was about 1 mm^3. Since the vapors of diesel fuel scatter light much more strongly than air, it is possible to probe for unmixed (partially mixed) diesel vapor in the outlet stream. Also, since scattering from fine droplets of fuel scatter light much more intensely than scattering from gases and vapors, it is possible to readily distinguish unvaporized fuel in the outlet steam. The ratio of the standard deviation in the scattered light signal divided by the time-mean scattered light signal is used as the indicator of the unmixedness of the fuel-air mixture. For running at high temperature (450 degrees C first stage, and 550 degrees C second stage) and high flow rate (SPP residence time of 4.5 ms), with the diesel fuel-air equivalence set at 0.5, the scattered light standard deviation over time-mean ratio was about 0.1. (The background ratio or the system, with only cold air flow through the laser test volume, was about 0.05.). The results indicate the ability to obtain an SPP outlet steam that is both well vaporized and well mixed for high flow, high temperature running of the SPP.

    d. CFD modeling of selected cases from the laboratory SPP runs of the 1-atm testing have been conducted. The CFD shows the velocity, temperature, and diesel vapor contours in the SPP. It also shows the fuel droplet behavior.

2. High-pressure evaluation:

    a. An industrial-scale SPP has been designed and fabricated by the Parker Hannifin Corporation, for high-pressure testing at Solar Turbines, Inc. (None of the AGTSR Subcontract 00-01-SR087 funding was used for the design and fabrication of the industrial-scale SPP.)

    b. A gas turbine combustor test cell at Solar Turbines, Inc. has been modified for high-pressure testing of the industrial-scale SPP. The modification was required because the SPP uses two inlet streams of air of different temperature. (The AGTSR Subcontract 00-01-SR087 paid for contractor alterations of the test cell and for flow control hardware specific to the SPP testing. This is the extent of the AGTSR Subcontract 00-01-SR087 costs at Solar Turbines, Inc.)

    c. CFD modeling of the industrial-scale SPP. The CFD shows the velocity, temperature, and diesel vapor contours in the SPP. It also shows the fuel droplet behavior.

The Staged Prevaporizing-Premixing Injector: High Pressure Evaluation

AGTSR Subaward No. 00-01-SR087

INTRODUCTION

The control of NO_x has become an ever important issue in the gas turbine and power generation industry as NO_x is a precursor to both photochemical smog and acid rain. The current method of controlling NO_x in a land based gas turbine engine is to operate the combustor in a lean premixed mode, thus lowering the flame temperature and taking advantage of the strong temperature dependency of NO_x formation caused by the Zeldovich mechanism. Prior to the 1990s, gas turbines used for both aircraft and land based power generation operated using a diffusion flame, which due to natural processes will burn chemically-correct. This in turn leads to very high flame temperatures and large NO_x production. Around 1990, the land based gas turbine industry installed lean premixed technology to control NO_x by operating the combustor at a $\phi \leq 0.6$. Currently, lean premixed technology for gas-fired land based gas turbines allows manufacturers to guarantee ≤ 25 ppmv of NO_x, some guarantee ≤ 15 ppmv and a few will go as low as 9 ppmv, all corrected to 15% O_2, dry. Diffusion flames continue to be used in aircraft engines due to the inherent instability problems associated with lean premixed combustion.

The current lean-premixed fuel of choice is natural gas, which is generally about 88 to 96% methane in the US (Lee, 2000). Gas turbine manufacturers have developed lean premixed combustion systems – an introduction to these combustion systems is found in Lefebvre (1999) section 9-7. However, the ever increasing use of natural gas raises the need for dual fuel operation of land based gas turbines. Occasionally, power plants can experience interruption to the natural gas supply causing the gas turbines to be run in a diffusion flame mode on liquid fuels such as diesel, typically with water injection for NO_x control. Water injection leads to increased capital cost and requires pre-treatment prior to injection into the gas turbine combustor.

The GTX100 engine uses a dry system for liquid fuels and the manufacture guarantees NO_x of less than about 25 ppmv (corrected to 15% O_2, dry) – Aigner et al. (1999). GE Power Systems reports achieving 75 ppmv of NO_x on diesel fuel in their dry low NO_x burner (Schorr, 1999). Research continues in this area, especially development work on dual fuel injectors.

The stage prevaporizer-premixer (SPP) developed by Lee (2000) is able to achieve less than 12 ppmv of NO_x burning No. 2 diesel and less than 5 ppmv of NO_x burning methane, all corrected to 15% O_2, dry. The staged prevaporizer premixer is a dry, lean prevaporized-premixed, dual fuel injector that represents advanced injector technology. In the work done by Lee (2000), the SPP was run in two different geometric configurations providing 17 or 24 ms for the short or long SPP, respectively. Industry criticism suggested the SPP operation be validated at residence times of about 5 ms to achieve acceptance by the gas turbine industry. The main focus of the present work is to verify the running of the SPP at short residence times and at the pressure levels of gas turbine engines.

SPP Concept: the idea central to the use of the SPP is staged injection with the first stage 100-200°C cooler than the second stage. The lower temperature first stage air is especially important when the injector works with a liquid fuel. If the temperature in the first stage is too high, auto-ignition might occur, on the other hand the higher temperatures lead to quicker vaporization of the fine liquid fuel spray. The extra step of vaporization required for liquid fuel potentially demands more residence time in the SPP. Estimates for vaporization of liquid fuels can be made using procedures outlined in either Lefebvre (1989) or Turns (2000). The work of Spadaccini and TeVelde (1982) found that the auto-ignition delay time is proportional to the inverse of pressure squared. For integration of any lean prevaporing-premixing injector system into a gas turbine engine the system must first atomize, then vaporize, and finally mix the lean fuel air mixture, all of this must be completed before auto-ignition occurs. The SPP uses air reduced below the temperature of the compressor discharge air to accomplish the vaporizing and initial mixing. Then, the second stage high temperature compressor discharge air is introduced into the SPP, completes the mixing process, and brings the SPP outlet stream to as high of temperature as possible. In the laboratory SPP of Lee (2000), the second stage air is introduced through several small holes that create high velocity jets. (There are a series of 16 holes (4 every 90° around the circumference of the SPP, oriented at 45° from the centerline of the main flow path) through which the second stage air jets are introduced into the main flow path.)

Cycle analysis work has been done by Campbell et al. (2002) with a model of the SPP integrated into multiple gas turbine combined cycles suggesting that the net cycle efficiency is minimally impacted by decreasing stage one air amount and temperature. Figure 1 shows a schematic of the SPP integrated into a Frame H combined cycle system. From the figure it can be seen the air exhausted from the compressor is split into two streams: one stream takes the high temperature air directly to the second stage of the SPP, and the other air stream is run through a heat exchanger and the air temperature is reduced for injection into the first stage of the SPP. The heat that is removed from the first stage air is then recovered in the HRSG on the steam side of the cycle. The work of Campbell et al. (2002) helped to provide insight when the test matrix was developed for the current experiments by suggesting that small amounts of first stage air, followed by the majority of the air injection in the second stage, would be the most likely operating scheme in a gas turbine cycle.

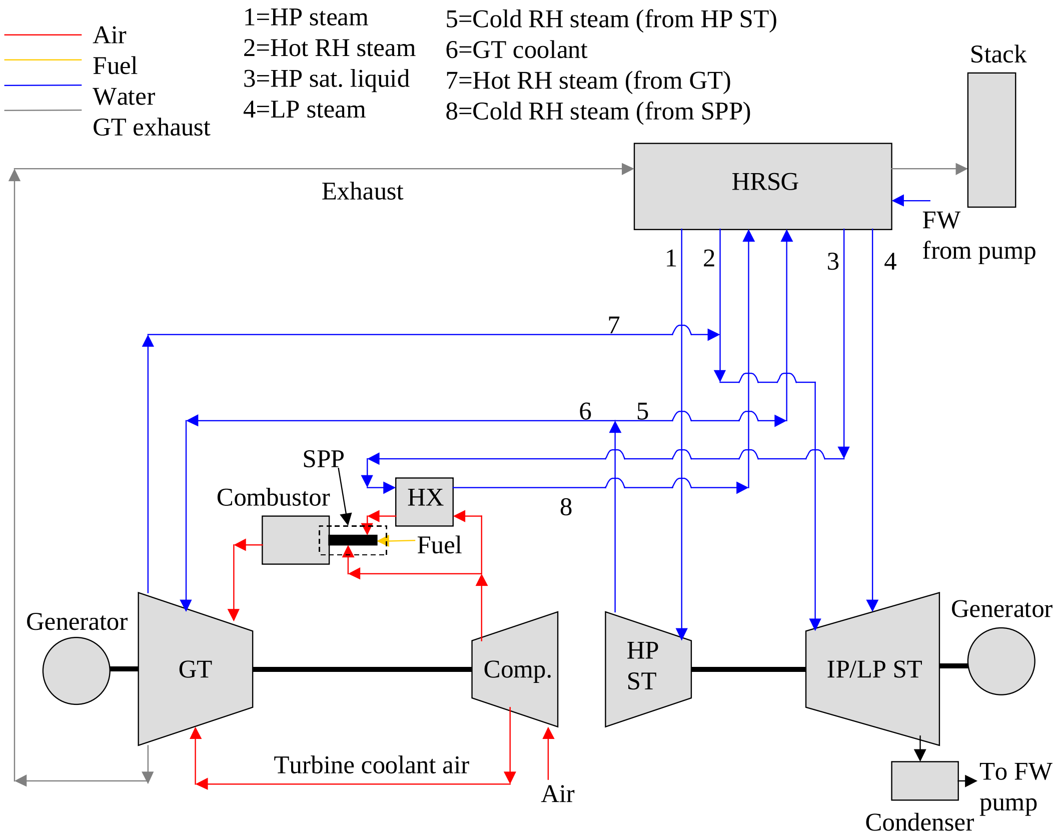

Figure 1: Schematic with the SPP integrated into a frame H combined cycle, taken from the work of Campbell et al. (2002).

This report describes both the laboratory SPP, operated at pressures of 1 to 2 atmospheres, and the industrial-scale SPP, for testing at gas turbine engine pressures. This information is provided in the following sections of the report:

- Laboratory SPP modified for this study.— experimental setup.
- Testing of the laboratory SPP, firing 16 cc jet-stirred reactor.
- Testing of the laboratory SPP, firing 64 cc jet-stirred reactor.
- Testing of the laboratory SPP, with the outlet stream examined by laser Rayleigh scattering.
- CFD modeling of the laboratory SPP.
- Description of the industrial SPP.
- Developing the test setup for the industrial SPP.
- CFD modeling of the industrial SPP.
- Conclusions and recommendations.

LABORATORY SPP MODIFIED FOR THIS STUDY – EXPERIMENTAL SETUP

The experimental rig used in this work is similar to the system described by Lee (2000). Figure 2 shows a schematic of the SPP with the JSR attached.

Heated air for stages one and two of the SPP is provided by electric convection-type heaters (Convectronics Model 007-10135). The heater temperatures and the “set point” temperatures (the stage one and two temperatures inside the SPP main flow channel) are monitored and controlled using a cascade temperature controller (Series 989, Watlow part # 989B-11FA-AARG) coupled to a Waltow DIN-a-mite SCR power controller. The first stage air after leaving the mass flow controller enters the first stage heater and then enters an annulus at the bottom of the SPP prior to the film atomizer that marks the entrance to the first stage of the SPP. Gaseous fuel is also introduced into this annulus prior to the film atomizer. The film atomizer consists of a thin circular tube feed with air from small holes in a circular plate. The small holes (approximately 0.015”) accelerate the flow into the first stage of the SPP. This also promotes quick liquid fuel vaporization and helps keep the liquid fuel spray off of the SPP first stage wall.

On centerline at the bottom of the SPP is a Nukiyama-Tanassawa type nozzle that was custom built for the work of Lee (2000). The liquid nozzle is a plain jet atomizer which provides a very fine spray. Lee (2001) estimates a 10 micron Sauter mean diameter (SMD) for this nozzle. See Lefebvre (1989) for discussion of the nozzle. The nozzle uses air cooling for all experimental data collected. The nozzle cooling air runs coaxially from the base of the nozzle to the tip where the spray is produced, and back to the nozzle base. This cooling air jacket prevents excessive heating of the liquid fuel from the stage one air that flows through the annulus surrounding the liquid nozzle. Unlike all the other air introduced into the SPP, the atomizer air is not heated. The beginning of the SPP second stage is considered to start at the taper in the main flow channel – this also marks the point where the staggered high velocity jets start to inject second stage air. There are 16 holes oriented 45º to the main flow path, four every 90º around the circumference of the SPP second stage. The second stage air enters through a similar heater control system as that used in the first stage. The air enters through a manifold that wraps the main flow channel of the SPP. At the end of the SPP a converging nozzle is used to accelerate the lean fuel and air mixture into the JSR where combustion occurs. The nozzle throat diameter used is 4mm. Larger nozzles were tried but the 4mm nozzle appears to be the largest that the JSR combustor could handle, otherwise the unreacted jet occupies too much of the combustor.

The JSR provides a high intensity combustion process in which the hot combustion products backmix onto the incoming high velocity fuel air mixture giving excellent flame holding and stability. The high intensity combustion causes the chemistry rate to significantly influence the reactor output. Although the JSR is designed as a well stirred reactor, spatial non-uniformities do exist within the reactor causing a distinct flame zone (the jet) surround by a distinct post flame zone (the recirculation zone). Exhaust products leave the JSR through the drain holes at the bottom of the combustor.

The JSR used in both this work and Lee (2000) has an internal volume of 15.8 cc. The flame temperature is monitored through an approximately 1/8" port in the side of the JSR using an R-type thermocouple (TC) with a ceramic sheath and ceramic coated tip identical to that described by Lee (2000). In the combustor it is estimated that only 30 degrees C is lost to radiation from the TC tip. The exhaust gas measurements are made using a quartz probe placed opposite the flame temperature TC, the quartz probe is this work used an unrestricted tip with an uncooled tip length of 1.625". Lee (2000) estimates an uncooled probe tip residence time of about 0.1ms and the cooled remainder of the probe has a residence time of 0.4 ms. Since this probe is at the same conditions (volume, mass flow throughput, and temperature) as run by Lee (2000), it can be assumed that the residence times estimated by Lee (2000) are again representative in this work. The emissions system is described later in this report.

A data logger (Fluke NetDAQ data logger) was used to monitor the flame temperature, the nozzle block temperature, the temperature of several TCs internally imbedded in JSR (these are used to determine when the combustor is thermal stable), and the temperature of the incoming air prior to the SPP film atomizer. All of the temperature data acquired by the Fluke NetDAQ logger was sampled at 1 Hz, and could be saved in the computer as a *.csv file for post test viewing. The first and second stage set point temperatures were monitored using the cascade temperature controllers.

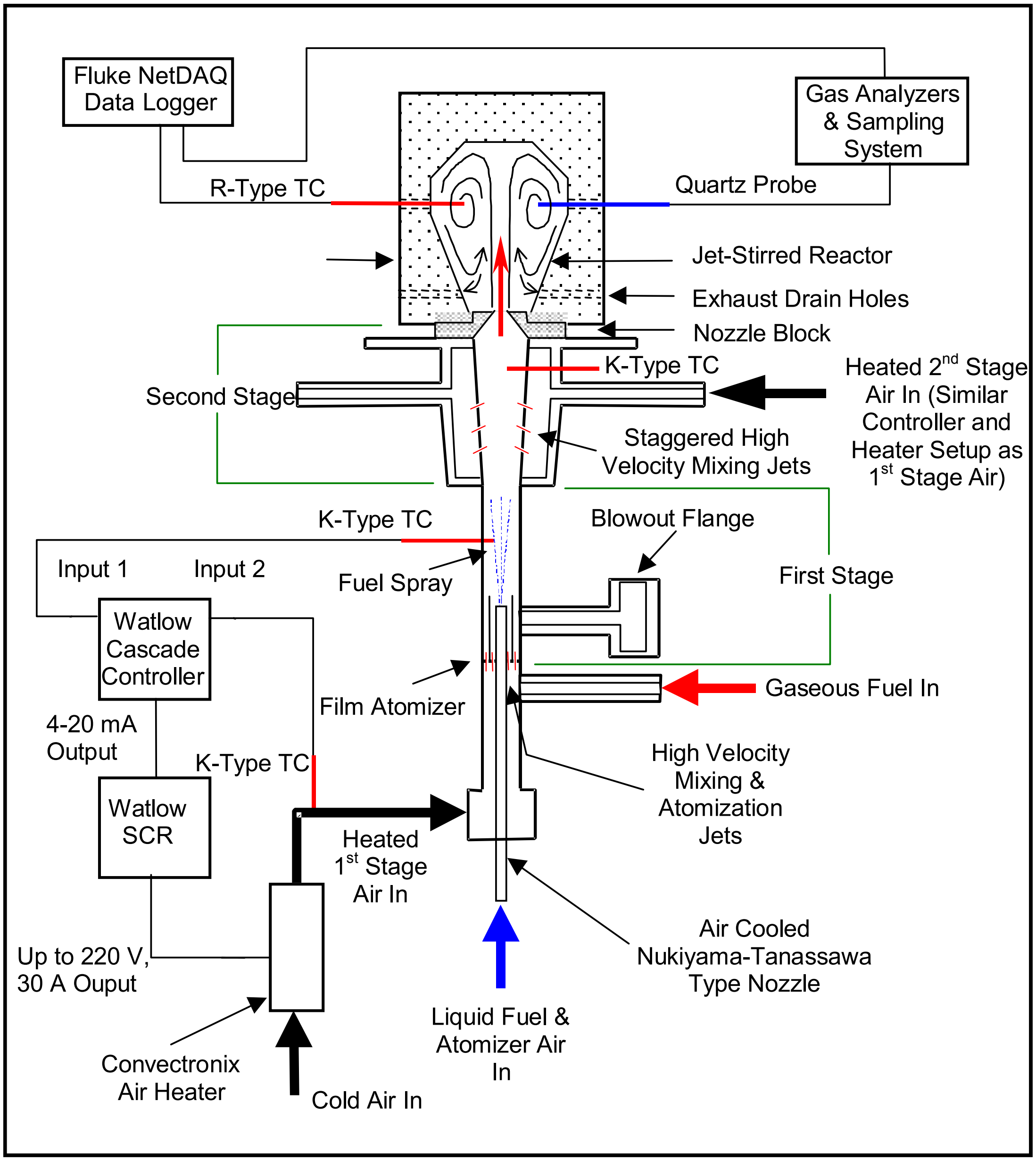

Figure 2: Schematic of the SPP/JSR experimental rig (taken from Lee, 2000, and modified).

Mass flow controls

Lee (2000) ran the SPP at relatively low mass flow rates. The first and second stage air mass flow controllers (mfcs) used by Lee (2000) each had a maximum range of 60 slpm (standard liters per minute). This would only allow for a doubling of the air mass flow rate since the standard case run by Lee (2000) used 30 slpm of air in each stage. The decision was made to re-work the current mfcs and recalibrate them for a maximum range of 100 slpm each. The air mfcs are Unit model UFC-3020. Since liquid fuels are the primary focus of this work, the gaseous fuel mfc was not recalibrated for a larger range and remains identical to that used by Lee (2000) – this did pose a small problem as methane combustion data were only obtained for air flows of 30 slpm to stage one and 100 slpm to stage two.

The liquid fuel flow was controlled in an ABB Fisher & Porter rotameter with a Parker Hannifin precision metering valve. The rotameter required the use of two different float materials, black glass for the light naphtha and stainless steel for the No. 2 diesel fuel. The system is identical to Lee's (2000) with the exception of the new rotameter and new metering valve. The fuel is pumped using nitrogen pressure, and calibration curves were generated using the "bucket and stopwatch" technique.

Heaters and temperature controllers

The basic heater configuration was maintained from Lee (2000), however, a few minor modifications had to be made to accommodate the high mass flows and high inlet temperatures that were desired in this work. In order to prevent un-repairable damage to the 1st stage heater it was insolated on a separate 120 V circuit with separate powerstat. Previously the first and second stage heaters were connected in parallel to a 220 V single phase circuit with a powerstat controlling the power to both heaters. The concern was that since all production data would be taken with a second stage air flow of 100 slpm, the powerstat voltage would have to be increased significantly to obtain the required power output in the second stage heater. This would have also increased the power in the first stage heater to unnecessarily high levels that could have damaged the heater. Therefore a separate powerstat connected to a 120 V circuit was used to power the first stage heater.

Pressure measurements

Static pressure measurements were made only using mechanical pressure gauges. The static pressure was monitored in the 1st and 2nd stages of the SPP, before the film atomizer, and before the heaters. The purpose of the pressure measurements before the film atomizer and the electric heaters was to try and characterize the effect these devices have on pressure loss. These measurements indicated about 3 -5 psid across the film atomizer and about 1-2 psid across the second stage inlet air holes and electric heater. As shown in Figure 1, the SPP integrated into a real gas turbine cycle would have to obtain the two different stage temperatures through the use of a heat exchanger rather than electrical heaters. In hindsight, it would have also been very helpful to have a static pressure tap at the nozzle throat at the entrance to the JSR. Simple isentropic gas dynamics calculations break down due to the back heating on the incoming fuel and air jet, therefore the combustor pressure had to be inferred from changes in SPP pressure indicating a change in back pressure or combustor pressure.

Emissions system

The emissions sampling system is identical to that of Lee (2000) with the exception of a different O_2 analyzer (Sybron/Taylor Servomex Model 570A). NO-NO_x, CO, CO_2, and O_2 were all obtained to determine the effectiveness of the SPP at controlling NO_x. The NO-NO_x analyzer (Thermo Electron model 10) is a chemiluminescent type. The CO analyzer (Horiba Model PIR-2000) and the CO_2 analyzer (Horiba Model VIA-510) are the non-dispersive infared type. The O_2 analyzer uses the paramagnetic method. The sample gases are drawn to the rack of analyzers using a metal bellows vacuum pump (Senior Flexonics, Inc., model MB-158). In order to prevent absorption of NO_2 in the gas sampling line the sample line is heated prior to an impinger set on ice that drops water out of the sample.

The span gases used for calibration of the NO_x analyzer consisted of a NO/NO_x and N_2 mix that contained 8.4 ppmv of NO_x, an excellent concentration for calibration due to the low NO_x levels that were obtained. The CO/CO_2 analyzers were spanned using a gas that consisted of 0.452 volume % of CO, and 6.99 volume % of CO_2, the balance of the span gas was N_2. No span gas was obtained for calibration of the O_2 analyzer. At the completion of each experimental run the analyzers were checked against the span gases for drift, if drift occurred it was then taken out of the raw data prior to analysis.

Fuels

The two liquid fuels, light naphtha and No. 2 diesel fuel, used in this work were also used by Lee (2000) allowing for no additional fuel analysis to be necessary. Table 1 shows a break down of important liquid fuel properties taken from fuel analyses obtained by Lee (2000).

Table 1: Liquid Fuel Summary Table Modified from Lee (2000).

Liquid Fuel	***Light Naphtha***	***Low Sulfur Diesel***
Molecular Formula	$C_{5.90}H_{12.45}$	$C_{13.77}H_{26.28}$
Boiling Range (K)	305 – 386	444 - 600
Molecular Weight	83.20	191.55
Specific Gravity	0.693	0.832
Reid Vapor Pressure (kPa)	75.1 – 82.0	< 20.7
C/H Molar Ratio	0.473	0.524
Fuel Bound Nitrogen (ppm by wt.)	< 1	124
Fuel Bound Sulfur (ppm by wt.)	9	195
LHV (MJ/kg)	51.45	43.11
Autoignition Temp. (K)	< 553	< 450

Initial Experiments with the Lee (2000) SPP

Initial testing was conducted with the as-received SPP-JSR system as used by Lee (2000). The goal of the present work was to test the laboratory SPP at flow rates considering larger than used by Lee (2000). The new flow rate goals were 55 slpm for stage 1, and 100 slpm for stage 2.

The initial experiments were encouraging as the SPP continued to give very competitive emissions numbers of less than 10 ppmv (corrected to 15% O_2, dry) when operated at the high flow rates on light naphtha fuel. As work continued, it was important to thoroughly inspect the SPP and make sure that there were no obvious leaks or signs of damage. The original SPP of Lee (2000) was designed to be run in both a “short” and “long” mode in order to directly vary the residence time by decreasing or increasing the injector volume. Several flanges were used to lengthen or shorten the SPP to achieve this affect. Figure 3 depicts the original SPP used by Lee (2000). Upon thorough inspection of the SPP, some signs of leakage were found in the SPP. Air entering the second stage manifold was not sealed off from the main flow channel, thereby allowing second stage air to bypass the small injection holes. While this was not a problem in Lee's work, at the increased flow rates of the new testing, which also increased the pressure within the SPP, premixed fuel and air were leaking out to the surrounding environment through some of the flanges.

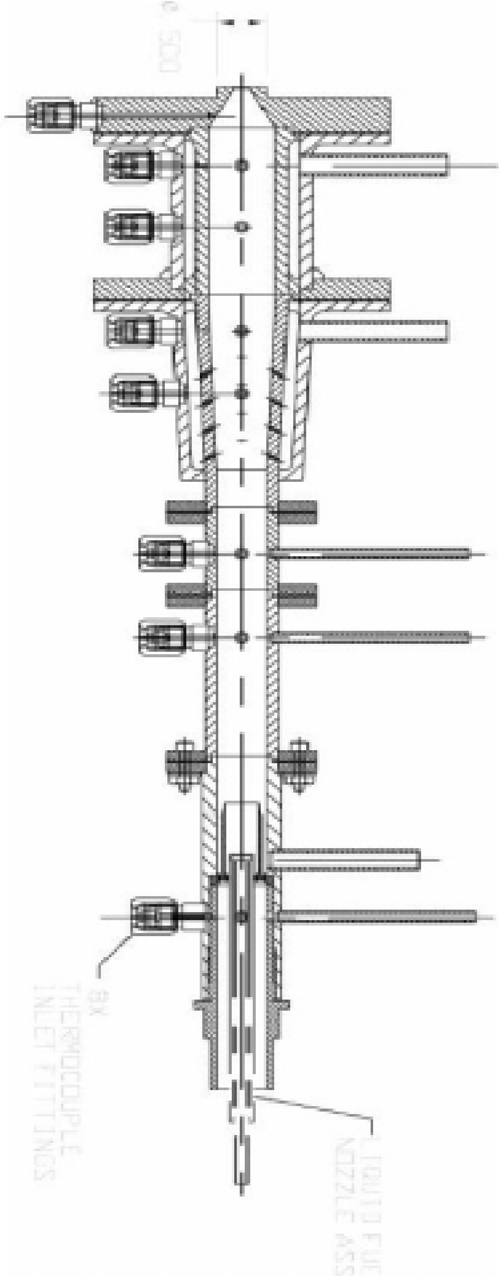

Figure 3: Long SPP developed by Lee (2000) and used for initial experiments.

New gasket materials were tried to see if the flanges could be sealed. In the end it was not possible to seal the leaks. This setback ended up being an excellent opportunity to revisit the design of the SPP and improve upon it. The volume could also be reduced, thus further reducing the residence time in the SPP.

Re-design of the SPP stage 2

The re-designed SPP second stage has many similarities to the original SPP. The taper angle and internal diameters before and after the taper were kept the same. The main changes involved thicker flanges to prevent warping, reduced length to reduce the residence time, and a new second stage manifolding technique to prevent leaks and force the second stage air to enter through the angular jets exclusively. Previously small bolts prone to breakage were used to connect the SPP together, these were changed at the second stage nozzle block flange, however the original hardware was retained at the bottom flange to match up with the first stage retained from the SPP used by Lee (2000). Three new nozzle blocks were built to couple to the second stage, however in the end the nozzle that had a 4 mm throat was used for all production data. This nozzle is dimensionally identical to that used by Lee (2000). Two other nozzles with a 6 mm throat were built, one for the current 16 cc JSR and one for a larger 64 cc JSR. The 6 mm nozzle coupled to the 16 cc JSR was tried in preliminary runs, however, difficulty was found with this configuration due to the large quantity of unreacted fuel and air allowed into the JSR relative the small combustor volume. The larger 64 cc JSR was used in later testing.

Figure 4 shows a section cut of the re-designed second stage. The bottom of the second stage connects to the flange that is noted in Figure 4. The second stage is considered to start at the beginning of the taper in the SPP that marks the beginning of the 16 holes used for second stage air injection. The first stage is considered to start at the film atomizer and ends at the beginning of the taper. There are 4 second stage air injection holes every 90° around the circumference of the SPP. Every 90° there is a slight stager in the injection holes along the length of the SPP to further promote mixing of the fuel rich mixture coming from the first stage. The injection holes separated by 180° on the circumference have the same location and spacing along the SPP length. The second stage holes are about twice the diameter (0.060 inches) of those used in the original Lee (2000) SPP in order to prevent excessive pressure loss.

For the re-design a simple can manifold was used for the second stage air injection into the SPP. The manifold is brazed in place along with the flanges. The manifold design creates an air tight seal with no need for gasketing. The arm seen in Figure 4 on the left of the section cut is the inlet of the second stage air. The second stage heater connects to this with both the SPP axis and the axis of the pipe heater running parallel to one another. A photo of the new SPP installed is shown in Figure 5. During the actual testing the SPP is covered with Kaowool insulation to prevent heat loss.

Figure 5 also shows the liquid nozzle injector coming in the bottom of the SPP first stage. In the foreground of the picture, to the left of the SPP center line the second stage heater can be seen. Near the lower right hand corner of the photograph the exit of the first stage air heater can be seen. The first stage air leaves the heater and is then routed through a 90º elbow entering the SPP perpendicular to the axis of the main flow channel. On the right side of the SPP two static pressure ports can be seen, and on the left side thermocouples (TC) are connected to monitor the SPP first and second stage temperatures. The top TC runs through a hole cross drilled all the way into the tapered nozzle. The gasket material used to seal the two flanges is Unifrax paper gasket material (Fiberfrax paper- 970A for nozzle block flange, 970J for JSR/nozzle block interface) which holds up very well in this relatively high temperature application.

Detailed drawings of the re-designed portion of the SPP are presented by Edmonds (2002). To give some idea of scale without thorough review of the drawings, the SPP nozzle block shown in Figure 4 has a diameter of 3”. The internal flow diameter of the first stage is 0.5” and the internal diameter at the exit of the second stage is 0.675”.

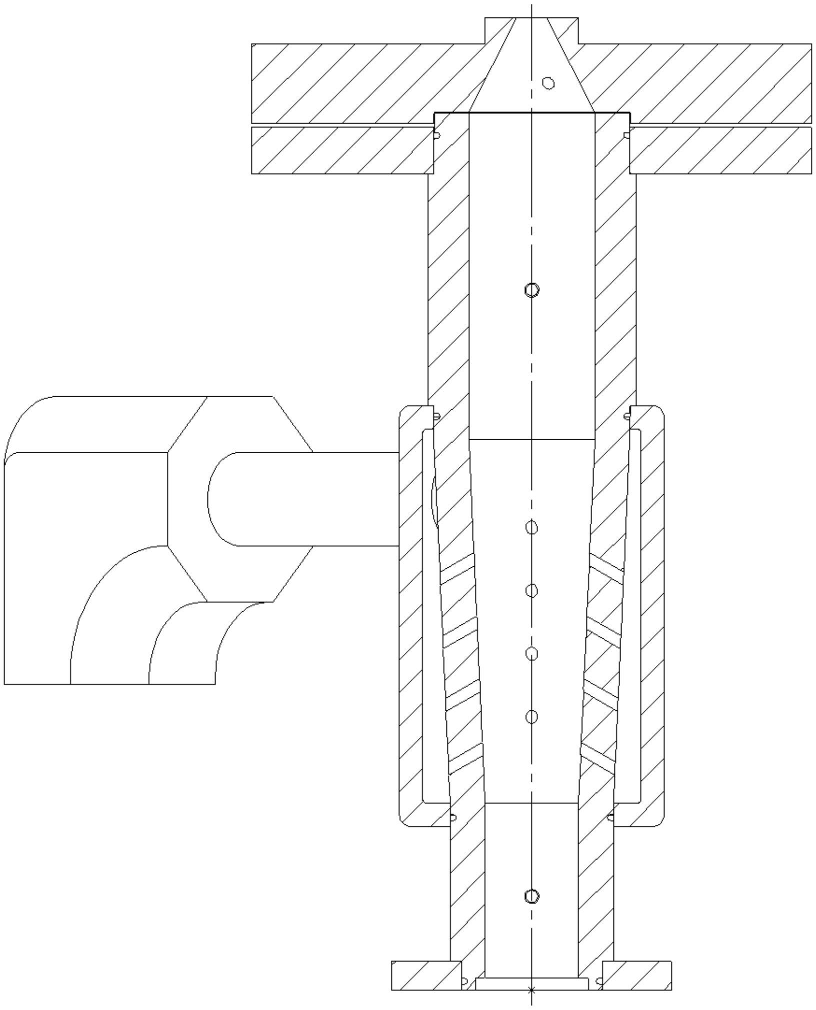

Figure 4: Section view of re-designed SPP second stage.

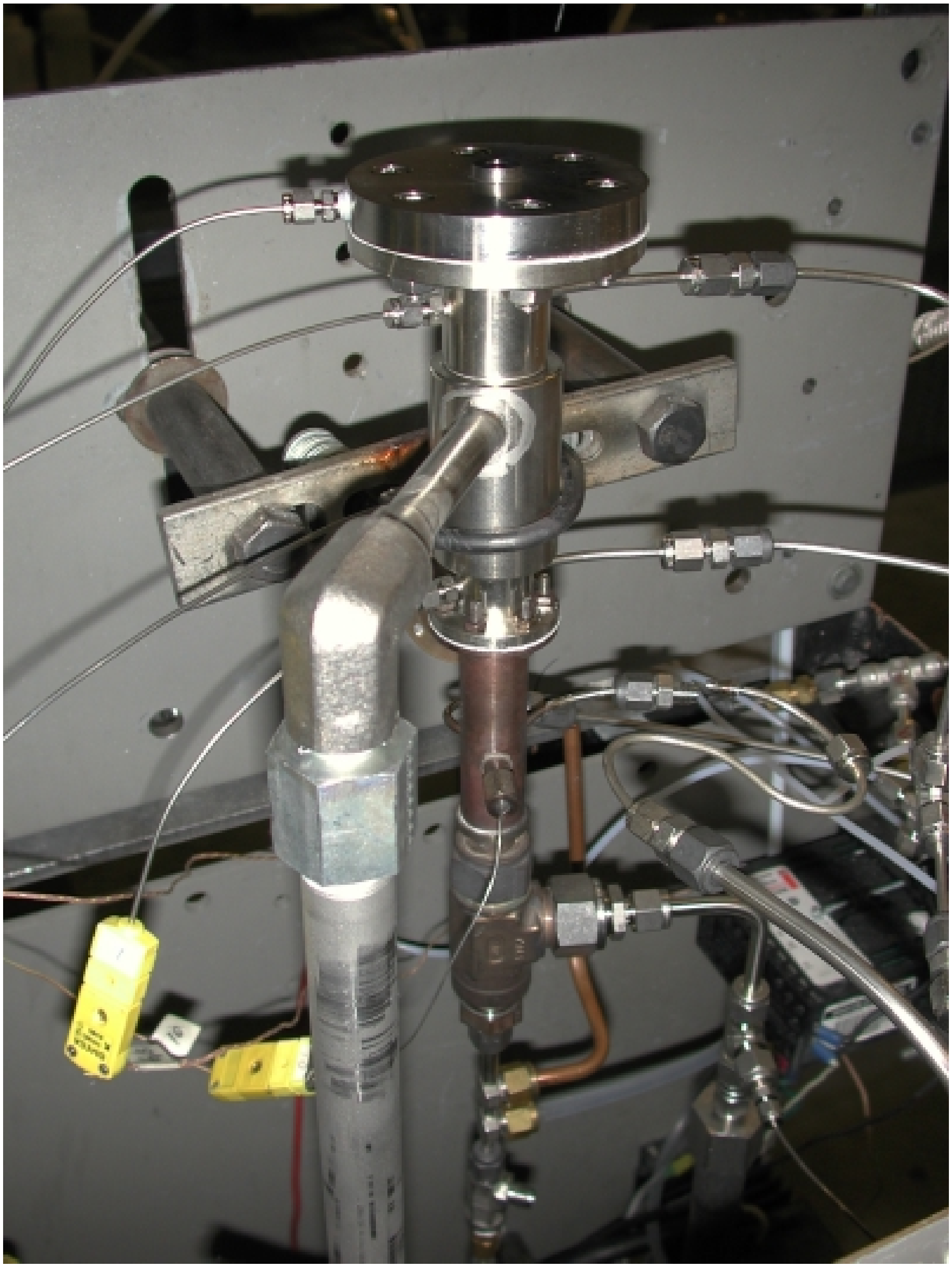

Figure 5: Photograph of SPP installed in combustion rig without insulation or JSR installed on top.

TESTING THE LABORATORY SPP, FIRING 16 CC JET-STIRRED REACTOR

Testing the modified SPP, firing the 16 cc JSR, is now described. The fuels used are methane, light naphtha, and commercial low sulfur diesel. The liquid fuels are the focus because of the more stringent requirements placed on the SPP by these fuels. When the liquid fuels are used, the SPP must first have good atomization, then quickly vaporize the fuel, and finally mix the fuel and air. Data were taken on methane in order to have a benchmark for comparison of the exhaust gas emissions from the liquid fuels. The desired data points for all fuels are shown in Table 2. The first stage air flow was 50 slpm (except 30 slpm for the methane experiments), and second stage air flow was 100 slpm. The set point temperatures of the two stages are changed in this work. The most interesting cases are at high temperature as these most closely represent gas turbine conditions.

Table 2: Desired first and second stage temperatures, overall fuel-air equivalence ratio and total residence time.

T_1 (deg. C)	150	250	300	400	450
T_2 (deg. C)	250	350	400	500	550
ϕ	0.5-0.7				
τ total SPP (ms)	10-18				

Methane results

The results for methane are shown in Table 3. The table shows how with varying stage one temperatures (T_1) and stage two temperature (T_2) the pressures, emissions, fuel-air equivalence ratio (ϕ), and residence times (τ) change. The flame temperature measured is also compared to the adiabatic flame temperature in Table 3. The notation used of 30/100 slpm refers to the air flows used in the first and second stages of the SPP, specifically in this case it refers to 30 slpm into stage one and 100 slpm into stage two. Note the total air flow in stage two is the sum of the inputs to stages one and two, i.e. 130 slpm in this case. Methane data were only taken at 30/100 slpm due to insufficient range on the gaseous fuel mass flow controller. It should be pointed out that in the cases were T_1=390°C and 405°C, the first stage heaters were being run at maximum. The low air flow rate caused the heaters to operate at their maximum allowable heater temperature, which does not allow for the desired temperatures of T_1=400°C and 450°C, respectively, to be reached. At the relatively low flow rate of the first stage air, there is insufficient heat transfer rate within the heater for the desired heat to be absorbed.

The emissions data for all fuels are discussed in the next section. The final equivalence ratios determined for all the results(including naphtha and diesel fuel) are the average of the fuel-air equivalence ratios obtained from both the CO/CO_2 and the O_2 exhaust gas measurements. Generally, the equivalence ratio calculated from the two independent emissions measurements varied by approximately 1-2% (relative). The reason that the equivalence ratio was not based on the mass flow rates is because it was about 8-10% less than the values obtained from the emissions samples, this was especially a problem when methane was the fuel. The methane fuel mfc was in need of recalibration. As should be expected the increase in temperature inside the SPP increased the pressure and decreased the residence times. The pressure is increasing with temperature inside the SPP because it is a constant volume steady flow device. The residence times in the SPP did not drop as low as anticipated due to the high internal pressures of about 11-14 psig (the pressures went as high as about 16 psig for the high flowrate conditions on the liquid fuels) within the SPP.

Table 3: NO_x, CO, fuel-air equivalence ratio, and residence times for methane at 30/100 slpm.

T_{JSR} (deg. C)	1490	1480	1480	1478	1478
$T_{\text{adiabatic equilibrium}}$ (deg. C)	1641	1629	1633	1608	1608
T_1 (deg. C)	150	250	300	390	405
T_2 (deg. C)	250	355	400	500	550
P 1st stage (psig)	11.25	11.75	12	12.75	13
P 2nd stage (psig)	11.75	12	12.5	13.25	13.5
NO_X at 15% O_2(ppmv, dry)	3.99	3.50	3.44	3.37	3.49
CO at actual O_2 (vol. %,dry)	0.244	0.217	0.207	0.171	0.150
ϕ from CO_2/CO	0.635	0.582	0.560	0.511	0.487
ϕ from O_2	0.659	0.602	0.588	0.516	0.492
ϕ average of CO_2/CO and O_2	0.647	0.592	0.574	0.513	0.490
V 1st stage (m^3)	8.00E-06	8.00E-06	8.00E-06	8.00E-06	8.00E-06
V 2nd stage (m^3)	2.04E-05	2.04E-05	2.04E-05	2.04E-05	2.04E-05
τ 1st stage (ms)	13.77	11.55	10.70	9.67	9.62
τ 2nd stage (ms)	8.75	7.40	7.04	6.33	6.01
τ total SPP (ms)	22.53	18.94	17.74	16.01	15.63
τ JSR (ms)	1.47	1.47	1.47	1.46	1.46

Naphtha results

Naphtha results are shown in Table 4 and Table 5 for 30/100 slpm and 50/100 slpm, respectively. The air heaters again had problems keeping the temperature up for the high temperature work, especially at the 30/100 slpm setting. It is apparent the heat of vaporization is also dropping the first stage temperature, for the high temperature cases, when the naphtha results of Table 4 are compared with the methane results of Table 3. At 30/100 slpm on methane the first stage reaches 390º C, but the same case shows naptha reaching only 370ºC, also for the highest temperature case the first stage air reaches 405º C and 390º C for methane and naptha, respectively.

Table 4: NO_x, CO, fuel-air equivalence ratio, and residence times for light naphtha at 30/100 slpm.

T_{JSR} (deg. C)	1475	1475	1480	1477	1478
T_1 (deg. C)	150	250	300	370	390
T_2 (deg. C)	250	350	400	500	550
P 1st stage (psig)	11.25	12	11.75	12	12.5
P 2nd stage (psig)	11.5	12.75	12	12.5	13
NO_X at 15% O_2(ppmv, dry)	5.06	5.05	4.93	5.49	5.54
CO at actual O_2 (vol. %,dry)	0.279	0.245	0.258	0.225	0.212
ϕ from CO_2/CO	0.60	0.56	0.53	0.49	0.47
ϕ from O_2	0.62	0.58	0.55	0.50	0.48
ϕ average of CO_2/CO and O_2	0.61	0.57	0.54	0.50	0.47
V 1st stage (m^3)	7.40E-06	7.40E-06	7.40E-06	7.40E-06	7.40E-06
V 2nd stage (m^3)	2.04E-05	2.04E-05	2.04E-05	2.04E-05	2.04E-05
τ 1st stage (ms)	14.98	12.51	11.36	10.25	10.14
τ 2nd stage (ms)	9.08	7.99	7.20	6.40	6.12
τ total SPP (ms)	24.06	20.50	18.56	16.65	16.26
τ JSR (ms)	1.45	1.45	1.44	1.44	1.44

Table 5: NO_x, CO, fuel-air equivalence ratio, and residence times for light naphtha at 50/100 slpm, both normal operation and data obtained during vapor lock are shown.

	Normal Operation					Vapor Lock
T_{JSR} (deg. C)	1480	1480	1480	1480	1478	1478
T_1 (deg. C)	150	250	300	388	420	426
T_2 (deg. C)	250	350	400	500	550	550
P 1st stage (psig)	13.25	13.75	14	15	15	15
P 2nd stage (psig)	13.75	14.25	14.5	15.5	15.5	15.75
NO_X at 15% O_2(ppmv, dry)	3.94	4.15	5.62	5.04	5.00	5.62
CO at actual O_2 (vol. %,dry)	0.292	0.252	0.240	0.191	0.175	0.183
ϕ from CO_2/CO	0.59	0.55	0.53	0.49	0.47	0.46
ϕ from O_2	0.61	0.57	0.54	0.50	0.48	0.48
ϕ average of CO_2/CO and O_2	0.60	0.56	0.54	0.50	0.47	0.47
V 1st stage (m^3)	7.40E-06	7.40E-06	7.40E-06	7.40E-06	7.40E-06	7.40E-06
V 2nd stage (m^3)	2.04E-05	2.04E-05	2.04E-05	2.04E-05	2.04E-05	2.04E-05
τ 1st stage (ms)	10.43	8.61	7.94	7.14	6.82	6.76
τ 2nd stage (ms)	8.59	7.35	6.86	6.19	5.81	5.86
τ total SPP (ms)	19.02	15.96	14.81	13.33	12.64	12.63
τ JSR (ms)	1.26	1.26	1.26	1.25	1.25	1.25

Table 5 shows results for naphtha combustion in both “normal operation” and “vapor lock” condition. Since naphtha is an easily vaporized fuel it is difficult to operate the plain jet atomizing nozzle under high temperature conditions. In the current SPP hot first stage air is brought in around the liquid nozzle which helps the atomization and vaporization process, but also can put too much heat into the liquid nozzle. The air flow path can be seen by re-visiting Figure 2 or Figure 3. In the case of naphtha at high temperatures the fuel starts to vaporize in the liquid nozzle which produces vapor lock in the nozzle. When this condition occurs the combustor receives short blasts of fuel and becomes very unstable making a repeated “pop-pop-pop” noise. This condition can be recovered from by quickly reducing the heater temperature. Vapor lock only occurred at the highest stage one temperatures that could be obtained In the current SPP rig configuration the naphtha liquid fuel tank allows for about 1.5 hrs of operation, given this constraint each condition was allowed to stabilize for approximately 10 minutes before data were taken and then the heater temperatures were adjusted.

Diesel results

The previous work of Lee (2000) found that No. 2 diesel fuel could not be vaporized in the SPP if the stage 1 temperature was below 180°C. Therefore all data for diesel were taken at a minimum temperature of 250°C, giving only four rather than five data points for each air flow rate. Once again the heaters are not able to provide the desired first stage temperature at the high temperatures. In the case of diesel fuel vapor lock is not a problem due to the resistance to vaporization that is characteristic of this fuel.

Table 6: NO_x, CO, fuel-air equivalence ratio, and residence times for low sulfur diesel at 30/100 slpm.

T_{JSR} (deg. C)	1477	1480	1478	1480
T_1 (deg. C)	250	300	365	389
T_2 (deg. C)	350	400	500	550
P 1st stage (psig)	11.75	12	12	12.5
P 2nd stage (psig)	12.25	12.5	12.5	13
NO_X at 15% O_2(ppmv, dry)	6.56	6.86	7.05	6.78
CO at actual O_2 (vol. %,dry)	0.268	0.241	0.240	0.225
ϕ from CO_2/CO	0.56	0.54	0.50	0.49
ϕ from O_2	0.57	0.55	0.52	0.51
ϕ average of CO_2/CO and O_2	0.57	0.54	0.51	0.50
V 1st stage (m^3)	7.40E-06	7.40E-06	7.40E-06	7.40E-06
V 2nd stage (m^3)	2.04E-05	2.04E-05	2.04E-05	2.04E-05
τ 1st stage (ms)	12.74	11.75	10.57	10.38
τ 2nd stage (ms)	7.91	7.39	6.43	6.16
τ total SPP (ms)	20.64	19.14	17.01	16.54
τ JSR (ms)	1.44	1.44	1.44	1.44

Table 7: NO_x, CO, fuel-air equivalence ratio, and residence times for low sulfur diesel at 50/100 slpm.

T_{JSR} (deg. C)	1476	1476	1480	1480
T_1 (deg. C)	250	300	400	436
T_2 (deg. C)	350	400	500	550
P 1st stage (psig)	14	14.5	15	15.1
P 2nd stage (psig)	14.75	15	15.75	15.9
NO_X at 15% O_2(ppmv, dry)	6.10	6.05	6.27	6.52
CO at actual O_2 (vol. %,dry)	0.218	0.209	0.230	0.222
ϕ from CO_2/CO	0.55	0.52	0.50	0.48
ϕ from O_2	0.56	0.54	0.52	0.50
ϕ average of CO_2/CO and O_2	0.55	0.53	0.51	0.49
V 1st stage (m^3)	7.40E-06	7.40E-06	7.40E-06	7.40E-06
V 2nd stage (m^3)	2.04E-05	2.04E-05	2.04E-05	2.04E-05
τ 1st stage (ms)	8.85	8.23	7.14	6.79
τ 2nd stage (ms)	7.53	7.03	6.28	5.92
τ total SPP (ms)	16.38	15.25	13.41	12.72
τ JSR (ms)	1.26	1.26	1.26	1.25

Analysis of data: effect of inlet air preheat on NO_X formation

The effect of air preheat on NOx data is analyzed first. The results are shown Figure 6. As can be seen there is little effect of inlet air preheat on the NO_x formation. Lee (2000) observed some decrease in NO_x with increasing preheat for methane. In this work the NO_x seems to be relatively flat at 3.5 ppmv (15% O_2 dry) for all methane cases except the first data point at 423K stage 1 air, and 523K stage 2 air preheat. It was theorized previously in the work of Rutar et al. (1998) that a decrease in NO_x could be explained because the decrease in equivalence ratio leads to less CH-radical and therefore less prompt NO_x.

It is also apparent from Figure 6 that the heavier the fuel is, the more NO_x is produced. This can be explained because the increase in carbon leads to more CO produced. A larger amount of CO oxidizing in the reactor leads to a larger amount of O-atom in the reactor, which promotes NO_x formation by the Zeldovich and nitrous oxide mechanisms (Lee et al., 2001).

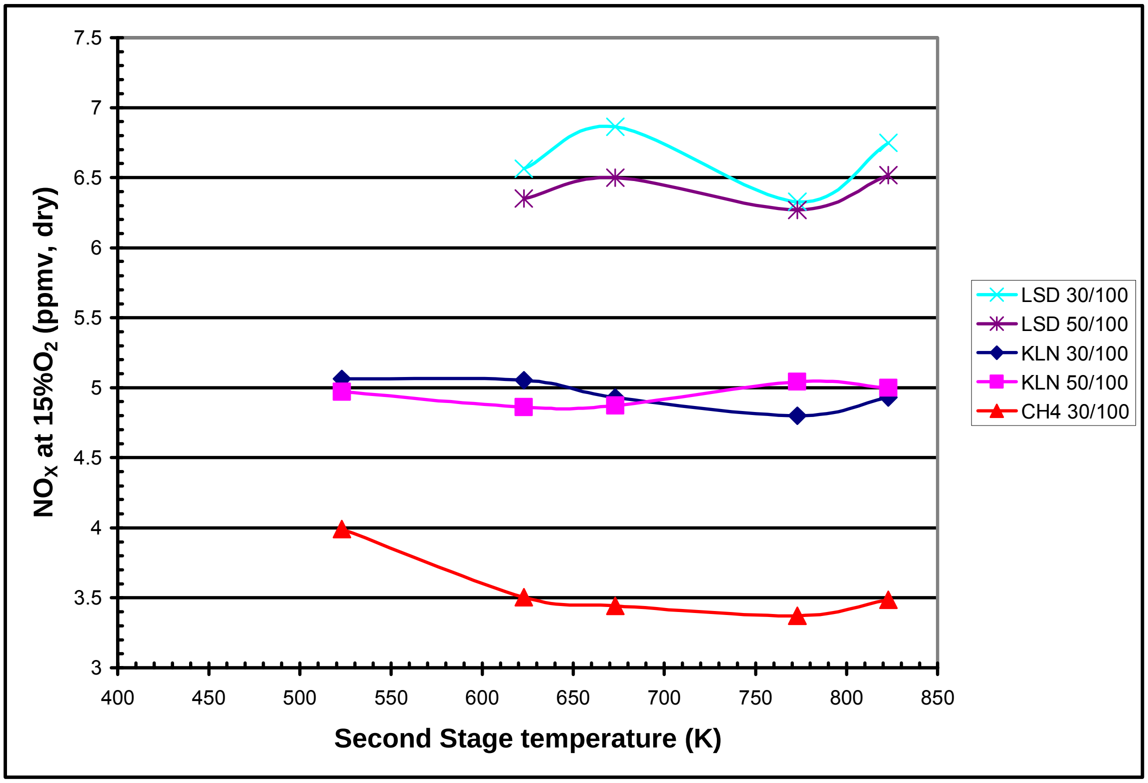

Figure 6: Effect of SPP outlet temperature (2nd stage temperature) on NO$_x$ formation for the three fuels. LSD is low sulfur diesel and KLN is light naphtha.

Analysis of data: comparison to the work of Lee (2000)

Comparison is made between the results of this study and those of Lee (2000). The NO$_x$ results at a standard condition of 250/355 (set points: 1st stage T=250 degrees C, 2nd stage T= 355 degrees C) are shown in Figure 7. As can be seen in all cases less NO$_x$ is produced in the current JSR. When considering NO$_x$ production it is important to consider both the radical pool in the combustor and the time that the mixture spends in the combustor. Both an increase in combustor residence time and an increase in radicals will lead to an increase in NO$_x$. The current work has an average combustor residence time of about 1.35 ms which is about 1 ms shorter than Lee (2000). From Figure 8 it can be seen that the CO does not increase dramatically over that of Lee (2000). Since the radical pool population behaves similarly to the CO pool, it follows that there may be little change in the radical pool within the JSR between these measurements and those of Lee (2000) . The O-atom radical is of primary interest because of its importance in NO_x formation – the small change in CO implies similar O-atom concentrations as those experienced by Lee (2000). Therefore, it appears the NO_x is lower because of a decrease in residence time.

It was expected that the CO would increase in the current experiments because of the short combustor residence times. However, less heat loss occurred in the current experiments, therefore a lower equivalence ratio was required to reach the standard flame temperature of 1790K. The leaner conditions in the current work should drive down the CO. However the short residence time of the current work appears to be offsetting this decrease making the results of this work and those of Lee (2000) essentially identical for CO.

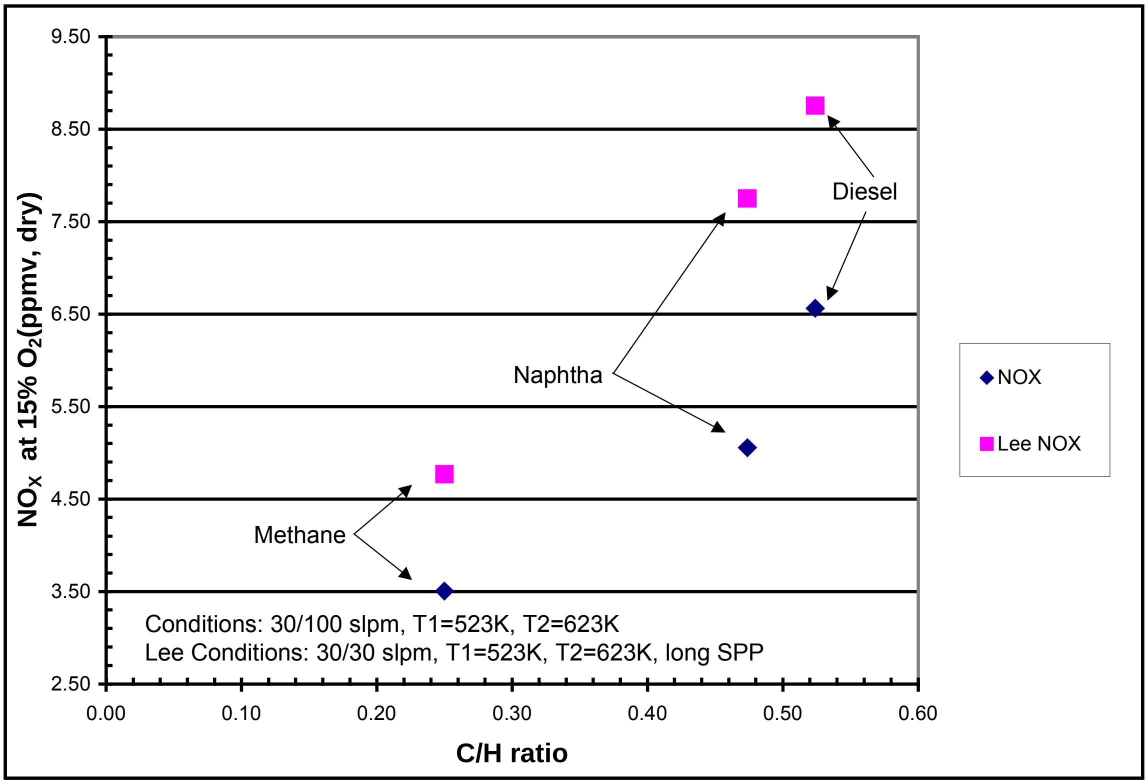

Figure 7: NO_x comparison for all fuels to the work of Lee (2000).

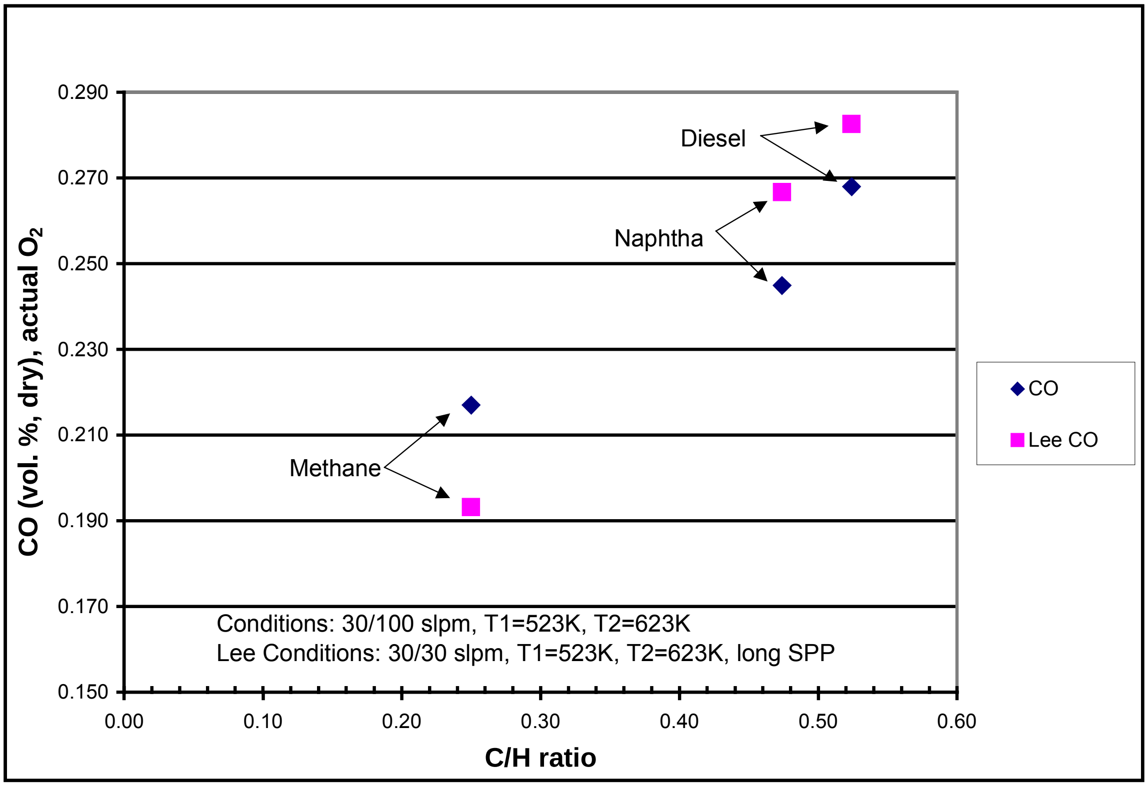

Figure 8: CO comparison for all fuels to the work of Lee (2000).

Analysis of data: combustor characteristics

The nominal combustor operating conditions are:

- T = 1790 K
- P = 1.2 atm
- Combustor residence time, $\tau = 1.35 \pm 0.1$ms

The Damköhler number (Da) was also estimated to better understand the specific combustion regime following the work of Abraham et al. (1985), which is reprinted in Turns (2000, Fig. 12.8). The Damköhler and turbulent Reynolds number are given below:

$$Da = \frac{\text{characteristic mixing time}}{\text{characteristic chemical time}} \qquad \text{Equation 1}$$

$$Da = \frac{\ell_0 {S_L}^2}{\alpha_u u'} \qquad \text{Equation 2}$$

$$\mathrm{Re}_T = \frac{u' \ell_0}{\nu_u} \qquad \text{Equation 3}$$

were ℓ_0 is the turbulent length scale, S_L is the laminar flame speed, α_u is the thermal diffusivity of the unburnt gas, u' is the root-mean-square velocity fluctuations, and ν_u is the kinematic viscosity of the unburned gas. The length scale used is the nozzle inlet diameter for the JSR, u' is taken as ten percent of the inlet jet velocity, and both the thermal diffusivity and kinematic viscosity are evaluated for air at the inlet conditions. The Damköhler number is only estimated for methane since no data are available to estimate S_L for naphtha and diesel. Using the method of Göttgens et al. (1992) to estimate S_L, Da is found for the SPP run at Lee's (2000) air flow rates of 30/30 slpm and also for the current air flow rate of 30/100 slpm. The results are shown in Table 8. The physical interpretation of both of these conditions is descriped as "flamelets-in-eddies" by Turns (2000). Flamelets-in-eddies are characterized by the parcels of burning fuel and air inside large eddies. The decrease in Da for the current conditions indicates the JSR has moved slightly closer to distributed reaction, which is the condition for a perfectly-stirred reactor (PSR).

Table 8: Damköhler number estimates for both 30/30 slpm of air [Lee's (2000) condition] and 30/100 slpm of air (current condition).

	30/30	30/100
Tu (K)	723	803
P (atm)	1	1.2
u' (m/s)	22.22	42.57
S_L (m/s)	0.95	1.22
Re_T	1156.18	2203.4
Da	1.45	1.23

Analysis of data: reactor scan plots

In order to further characterize the reactor, emissions and temperature data were taken as a function of radial position in the JSR. The data from these experiments are plotted below. During these tests the JSR was run at its standard temperature of 1790 K, and then the sample probe was traversed from the combustor wall at about r = 12mm, into the center of the JSR. In order to obtain the temperature scan plots the sample probe was removed from the JSR as the fuel and air were held constant, then the temperature scan was commenced. As can be seen in Figure 9 the reactor temperature is less than 1790 K at the standard TC location of 8 mm, the actual temperature at this radial location is between 1750K and 1765 depending on the fuel. This temperature decrease is likely caused by a change in the aerodynamics within the reactor. Emission scan plots for methane are complete, however when data were taken on diesel the sample probe encountered the un-burnt fuel and air jet at about r = 4 mm. When this partially cracked mixture of fuel and air was pulled through the sample probe tar began to form due to the rapid decrease in temperature as the sample reached the water jacket used for cooling the quartz probe. This effect leaves the emissions results in doubt for r < 4 mm. After this problem was encountered no scan data were taken for naphtha at r < 4mm as tar formation was beginning to occur also for this fuel.

Figure 10 shows the NO_x results for all three fuels, both the 15% O_2 corrected results and the "as measured" results are shown. In all cases the NO_x is relatively flat for $r \geq 5$ mm in the flame zone. The NO_x drops off as expected in the unburnt center jet. Figure 11 shows the CO, CO_2, and O_2 results for all three fuels. Note the increase in O_2 for methane near the JSR wall. Also, note the CO, CO_2, and O_2 for $r \leq 4$mm for diesel are suspect because of the tar formation in the sample probe. The CO profile shows the peak CO at a larger radius when methane is the fuel versus both liquid fuels. This is expected since methane is a relatively slow burning fuel.

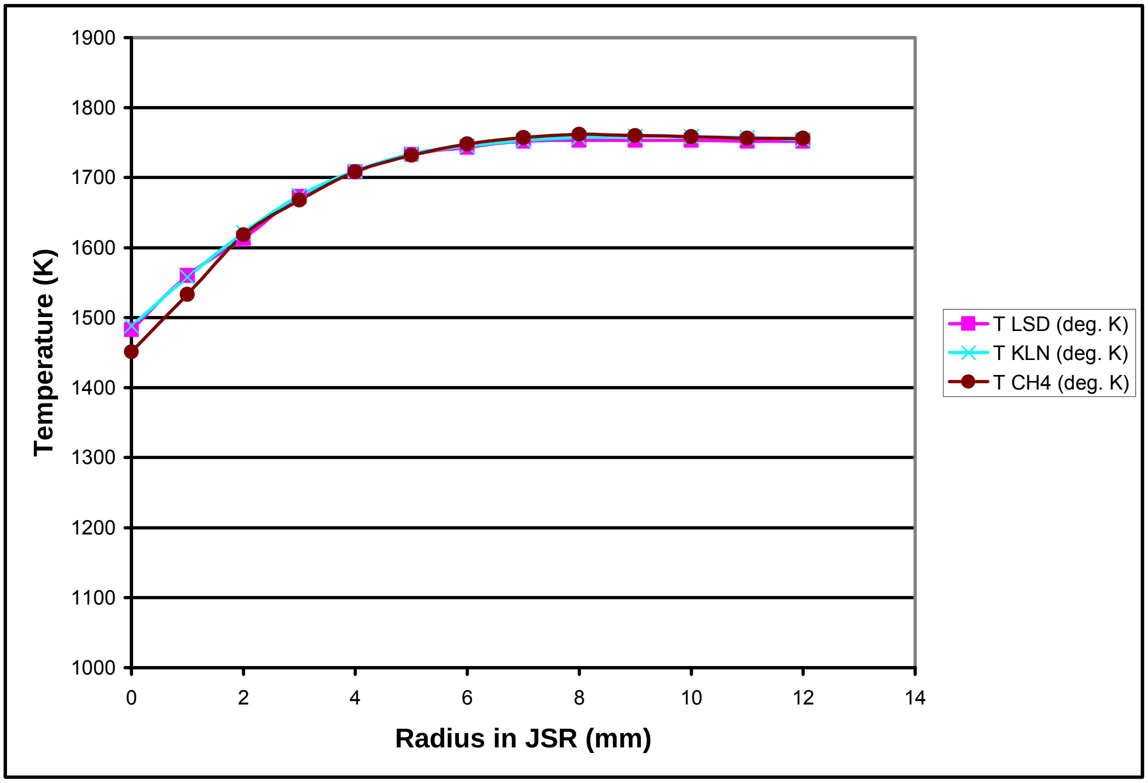

Figure 9: Temperature radial profile in JSR for all three fuels.

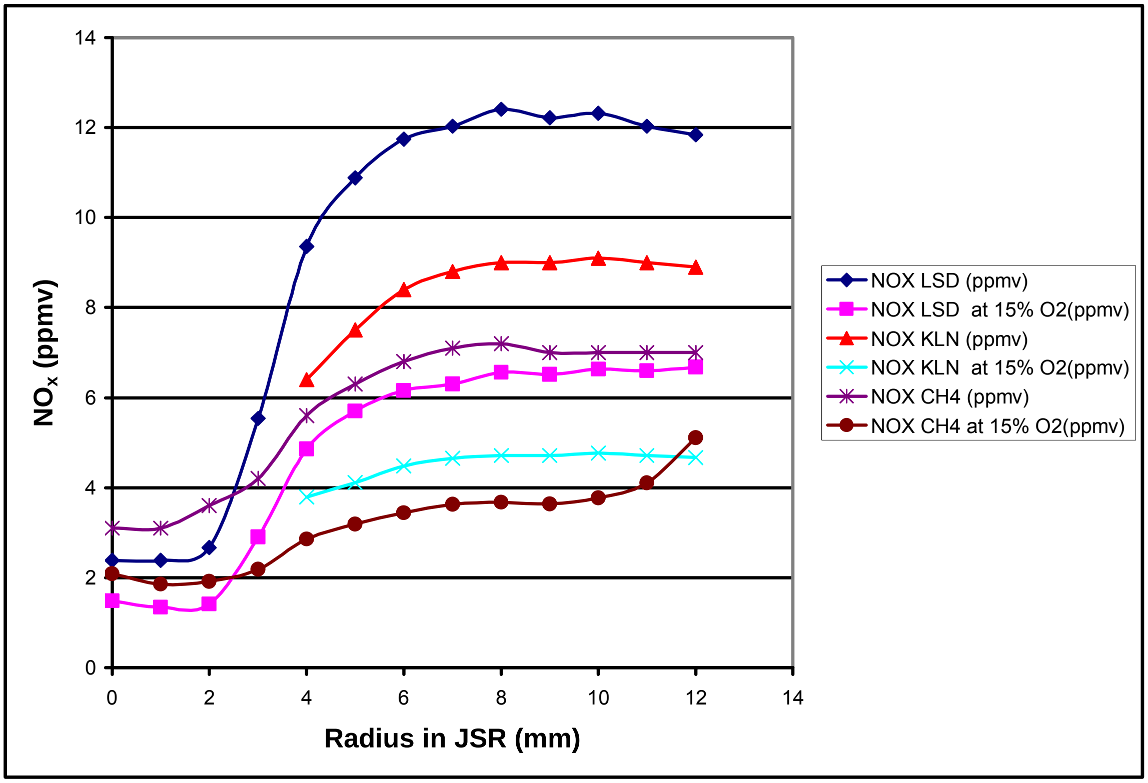

Figure 10: NO_x radial profiles (dry basis) for all three fuels shown at both at 15% O_2, and as measured.

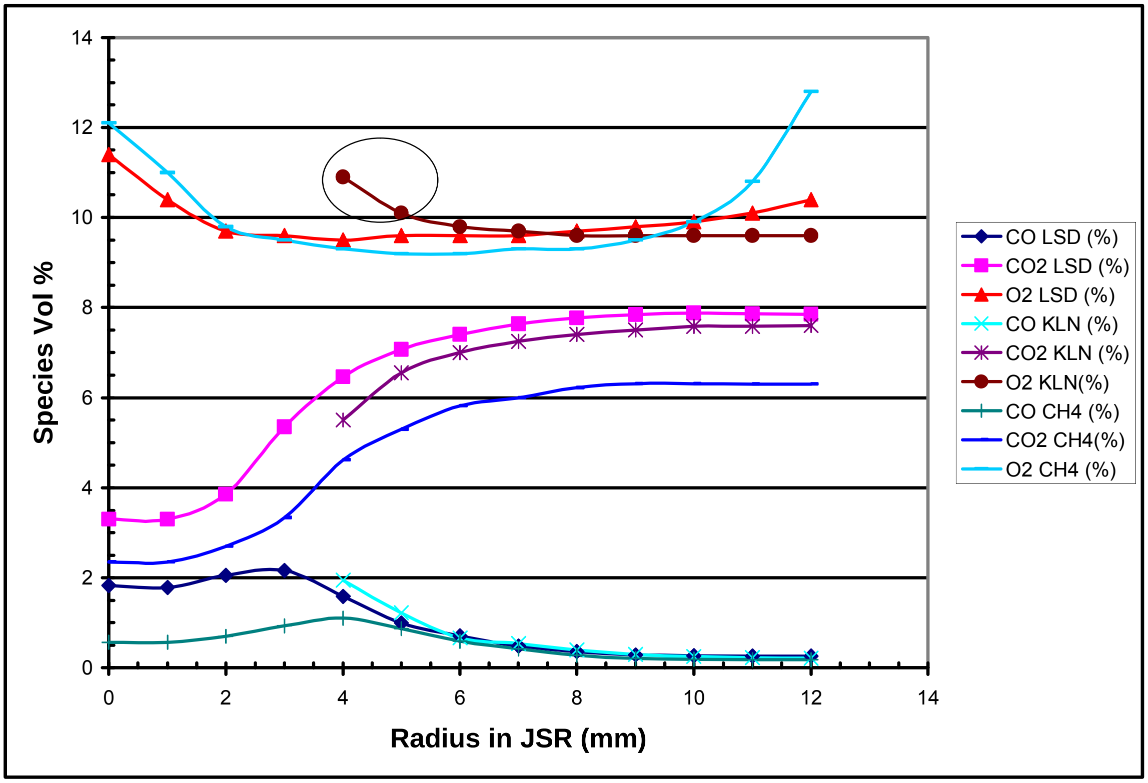

Figure 11: CO, CO_2, and O_2 radial profiles for all three fuels (dry basis). [The oval around the O_2 result for KLN indicates a potential error in the tear reading for the measurement.]

TESTING THE LABORATORY SPP, FIRING 64 cc JET-STIRRED REACTOR

The testing with the SPP coupled to the 16 cc JSR was limited by two factors: the backpressure created by the 4 mm nozzle and the blowout of the JSR (when its residence time was dropped below 1 ms).

In order to test the SPP at large flow rates and thus short residence times, two replacements were made:

1. The 6 mm nozzle replaced the 4 mm nozzle.
2. The 64 cc JSR replaced the 16 cc JSR.

With these changes it was possible to test the SPP-JSR system at the maximum air flows and temperatures in the SPP possible with the hardware:

- Total air flow of 205 slpm.
- Second stage temperature of about 575 degrees C.

Under these conditions it was possible to run the SPP at residence times of 5.6 to 7.9 ms. Pressure in the SPP was reduced to 4-7 psig. The residence time of the JSR was 3.6 to 4.8 ms.

Two fuels were used in these tests: low-sulfur diesel and commercial propane.

Results are given in Table 9. Because of the reduced surface-volume ratio of the 64 cc reactor compared to the 16 cc reactor, the 64 cc reactor could be run at a lower fuel-air equivalence ratio than the 16 cc reactor in order to reach the 1790 K corrected combustion temperature. (The JSR temperatures listed in Table 9 are raw data, uncorrected for the thermocouple radiation temperature loss of about 30 degrees C.)

For running on diesel fuel, the NOx emission was 7-8 ppmv (15% O_2 dry). These values fall between the 16 cc JSR data of the previous section and the data of Lee (2000).

Throughout these tests, the SPP-JSR system ran well, and yielded a low emission of NOx. It is concluded that the SPP is capable of providing low NOx emissions when used to vaporize and premix diesel fuel at residence times as short as 5-6 ms and temperatures of about 400 degrees for stage 1 and over 550 degrees C for stage 2.

Table 9: Results of testing of laboratory SPP firing 64 cc jet-stirred reactor

Measurement	**Units**	**test 1**	**test 2**	**test 3**	**test 4**	**test 5**	**test 6**	**test 7**	**test 8**	**test 9**	**test 10**	**test 11**
Atomizer air	**slpm**	5	5	5	5	5	5	5	5	5	5	5
Atomizer air	**kg/s**	1.00E-04	1.00E-04	1.00E-04	1.0E-04	1.0E-04	1.0E-04	1.0E-04	1.0E-04	1.0E-04	1.0E-04	1.0E-04
1st stage air	**slpm**	50	50	50	90	100	100	100	99.5	99.5	99.5	100
1st stage air	**kg/s**	1.00E-03	1.00E-03	1.00E-03	1.8E-03	2.0E-03	2.0E-03	2.0E-03	2.0E-03	2.0E-03	2.0E-03	2.0E-03
2nd stage Air	**slpm**	100	100	100	100	100	100	100	100	100	100	100
2nd stage Air	**kg/s**	2.00E-03	2.00E-03	2.00E-03	2.0E-03	2.0E-03	2.0E-03	2.0E-03	2.0E-03	2.0E-03	2.0E-03	2.0E-03
1st Stage T	**°C**	400	400	401	352	338	334	340	358	378	385	392
2nd Stage T	**°C**	521	522	523	500	496	502	501	525	557	557	572
Propane	**slpm**	8.72	8.72	0	0	0	0	10	10	10	10	10
Propane	**g/s**	0.086	0.086	0.000	0.000	0.000	0.000	0.099	0.099	0.099	0.099	0.099
Low-S Diesel	**rot. reading**	0	0	128	142	146	145	43	34	23	24	22.3
Low-S Diesel	**g/s**	0.0000	0.0000	0.0975	0.1196	0.1264	0.1247	0.0137	0.0099	0.0066	0.0068	0.0064
P_{SPP}	**psig**	4	4		5.75	6	6	6.2	6.5	6.5	6.5	6.6
Nozzle T	**°C**						560	554	560	575	578	585
JSR T	**°C**	1483	1483	1482	1485	1483	1480	1483	1483	1480	1480	1487
Calculations	**Units**	**test 1**	**test 2**	**test 3**	**test 4**	**test 5**	**test 6**	**test 7**	**test 8**	**test 9**	**test 10**	**test 11**
equivalence ratio	**by mass**	0.43	0.43	0.36	0.43	0.45	0.44					
residence time 1	**sec**	0.0043	0.0043	0.0035	0.0030	0.0028	0.0029	0.0028	0.0028	0.0027	0.0027	0.0026
residence time 2	**sec**	0.0037	0.0037	0.0029	0.0033	0.0032	0.0032	0.0032	0.0031	0.0030	0.0030	0.0030
SPP total time 1+2	**sec**	0.0079	0.0079	0.0064	0.0063	0.0060	0.0060	0.0060	0.0059	0.0057	0.0057	0.0056
JSR res time	**sec**	0.0048	0.0048	0.0048	0.0038	0.0036	0.0036	0.0036	0.0037	0.0037	0.0037	0.0036
Emissions	**Units**	**test 1**	**test 2**	**test 3**	**test 4**	**test 5**	**test 6**	**test 7**	**test 8**	**test 9**	**test 10**	**test 11**
CO	**%**	0.092	0.101	0.125	0.139	0.142	0.14	0.111	0.105	0.099	0.099	0.098
CO2	**%**	6.86	6.85	7.57	7.49	7.46	7.36	6.82	6.58	6.37	6.37	6.35
O2	**%**	9.7	9.8	9.9	9.9	9.9	10.1	9.9	10.2	10.5	10.5	10.6
NOx	**ppmv**	11	11	14.5	14	13.5	13	10	9.5	9.5	9.5	10
NOx 15% O2	**ppmv@15%**	5.8	5.8	7.8	7.5	7.2	7.1	5.4	5.2	5.4	5.4	5.7

TESTING THE LABORATORY SPP, WITH THE OUTLET STREAM EXAMINED BY LASER RAYLEIGH SCATTERING

Laser Rayleigh scattering setup and considerations

The laser Rayleigh scattering (LRS) setup used measures the scattering signal from a finite volume as a function of time. This technique is especially useful for binary mixtures of gases when the two gases undergoing mixing have vastly different scattering cross sections. Based on the refractivity of octane (C_8H_{18}, which is the heaviest hydrocarbon listed in Gardiner et al., 1981), the scattering cross section ratio of octane to air is roughly 100/1, while Espey and Dec (1997) used a ratio of diesel to air as 305/1. These ratios imply that it is possible to clearly differentiate air from diesel fuel vapor in the LRS measuring volume. The pertinent equations are as follows:

$$I_{scattered} = I_{incident} K n \quad x_i \sigma_i \qquad \mathrm{x_i} = 1$$ Equation 4

$$n = \frac{P}{kT} \qquad \mathrm{k} = \frac{\mathrm{R_u}}{\mathrm{N_{avogadro}}}$$ Equation 5

The terms in the equations are:

I = intensity of light
K = optical system constant
n = total number density as molecules per volume
k = Boltzmann constant
x = species fraction
σ = species scattering cross section

The above equations display the relevant parameters measured at the test volume. For the present work, P is always 1 atmosphere, the species scattering cross sections are constant, and the collection optics solid angle, transmission and efficiency (embedded in K) are constant. Temperature does change, however, as do the fuel and air concentrations (with equivalence ratio). A leaner or hotter mixture reduces the scattering signal while a richer or colder mixture increases the scattering signal. Equation 4 describes molecular scattering only, particles or droplets will scatter much more strongly and will be clearly noticeable. Scatters smaller than about 50nm (<< 514 nm) will behave as molecules, while larger scatters will behave as Mie scatterers – many orders of magnitude stronger than molecular scattering. In the time trace data shown below, droplets are noticeable as spikes of the signal.

The collection optics system is designed to capture the test-volume-averaged scattering signal and process the light signal onto a photomultiplier tube. Figure 12 shows a schematic of the collection optics system and relevant geometry. Similar optical setups were used by Dibble and Hollenbach (1981) and Yee (1982). Laurendeau (1991) provides descriptions of scattering techniques.

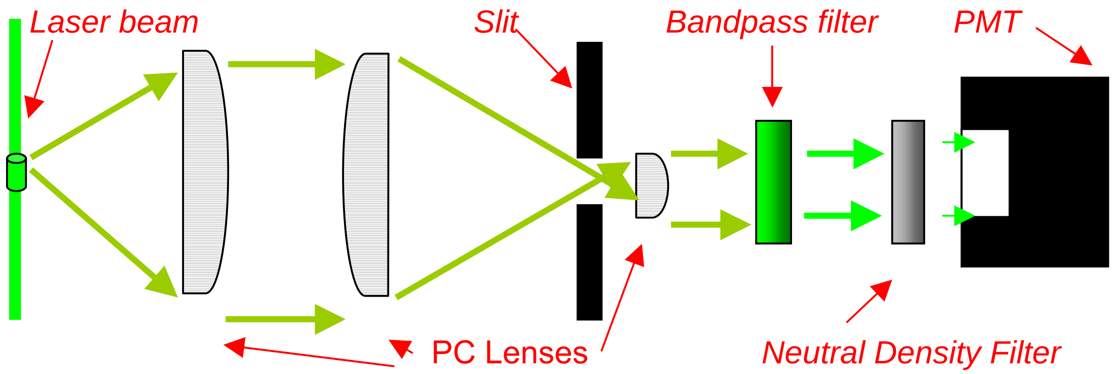

FIGURE 12: Schematic of collection optics system.

The slit in Figure 12 is used to limit the laser beam image that is projected onto the front face of the slit. This, along with the beam diameter, defines the measurement volume in terms of a cylinder. This cylindrical volume can be adjusted through the focal length of the lenses and the width of the slit, for finer or coarser measurements. The bandpass filter is used to isolate the laser wavelength of 514 nm, while the neutral density filter is used to reduce the signal reaching the PMT, to keep the signal on scale

SPP setup

The SPP injector, along with the 1st and 2nd stage air heaters and controllers, were not altered from the testing of the SPP described in the previous sections of this report, but a new test stand was built to facilitate the optical measurements. The SPP was mounted on an adjustable uni-strut frame, and rotometers were installed to measure the airflow rather than the MFC's used in the previous work. The JSR and accompanying nozzle were removed, since the LRS measurements do not involve combustion. This allowed nearly 1 atmosphere pressure to be attained inside of the SPP stages, which in turn helped to lower the residence time into the 4-7 ms range. Equations 6 and 7 show the functional dependence of the residence time.

$$\rho = \frac{P}{RT} \qquad R = \frac{R_u * \dfrac{\dot{m}_i}{MW_i}}{\dot{m}_i} \qquad \text{Equation 6}$$

$$\tau = \frac{\rho V}{\dot{m}_i} = \frac{P * V}{T * R_u * \dfrac{\dot{m}_i}{MW_i}} \qquad \text{Equation 7}$$

The stoichiometric fuel / air ratio for No. 2 diesel is nominally 0.069 (kg_{fuel} / kg_{air}). Using the molecular masses, the fuel / air mol ratio is about 0.01. There are about 100 molecules of air (O_2 and N_2) per "molecule" of diesel vapor.

Procedure

The laser beam is directed across the outlet of the SPP, a few mm downstream of the outlet. The scattered light is collected perpendicular to the laser beam, through a solid angle of about 0.4 sterradian. The scattering signal is measured as a function of time using the photomultiplier tube, Fluke Combiscope and data acquisition computer. Data are taken in the form of "snapshots" which capture the oscilliscope screen and record the data points. The time-length of a snapshot is 0.2044 seconds, containing 512 points with time intervals of 0.0004 second. This time interval is deemed appropriate to investigate the mixing without significantly succumbing to noise. The baseline noise standard deviation is about 5% of the mean signal. Temperature fluctuations, diesel vapor concentration fluctuations, droplets of diesel fuel, laser power fluctuations, and electronic noise all add fluctuations to the scattering signal, thereby increasing the ratio of standard deviation over time-mean of the scattering signal. The time data are recorded into a spread sheet, where the means and standard deviations of the signal "snapshots" are calculated and tabulated.

There are several parameters which were adjusted during the LRS diagnostic testing of the SPP, including airflow rates, equivalence ratio, and the 1st and 2nd stage temperatures. These parameters were adjusted to replicate the SPP conditions of the earlier work, and to extend the SPP flow to low residence times approaching 4 ms. Table 10 gives the LRS test matrix. Note the residence time of the SPP ranges from 4.3 to 10.5 milliseconds.

TABLE 10: Test matrix of SPP conditions tested with the LRS diagnostic.

slpm	slpm	slpm	°C	°C	by mass	ms
3.5	54	54	350 - 450	350 - 550	0.5	6.8 - 9.3
4.1	71	71	350 - 450	350 - 550	0.5	5.2 - 6.5
4.1	85	85	350 - 450	350 - 550	0.5	4.5 - 5.6
3.9	54	54	350 - 450	350 - 550	0.6	6.8 - 8.6
3.6	71	71	350 - 450	350 - 550	0.6	5.2 - 6.6
3.6	85	85	350 - 450	350 - 550	0.6	4.3 - 5.6
5	32	85	324 - 387	350 - 600	0.5	8.6 - 10.5
5	44	85	350 - 438	350 - 600	0.5	6.7 - 8.5
5	53	85	350 - 450	350 - 600	0.5	5.9 - 7.6
5	85	85	350 - 446	350 - 600	0.5	4.4 - 5.6

Results

The plots on the following pages are of two types. The first are the time traces of scattering signal – reproductions of the oscilliscope screen – while the second type depict the time-mean and standard deviation data as a function of the parameters. All temperatures listed refer to the stage set point temperatures, rather than to the air inlet temperatures. The air inlet temperatures are hotter than the set point temperatures – about 20 degrees C hotter for stage 1 and about 10 degrees C hotter for stage 2. The stage 2 temperature is close to the mean outlet temperature of the SPP. The air flow-rates are included in units of slpm.

Figures 13, 14, and 15 show representative time traces of the scattering signal. Stronger scattering corresponds to a larger negative value of the signal recorded – that is, as plotted, the scattering signal is downward increasing.

Figure 13 shows the scattering for the leanest phi tested (0.5) at the largest flow rates run. The residence time of the SPP ranged from 4.5 to 5.6 ms, with the shortest time corresponding to the highest temperature case.

With increasing temperature, the time traces in Figure 13 show decreasing scattering intensity and decreasing fluctuations. The low temperature cases, with low atomizer air flow rate, show substantial noise in the scattering signal, indicative of some droplets reaching the outlet of the SPP. Low temperature and low atomizer air are most challenging for attaining a well vaporized outlet stream.

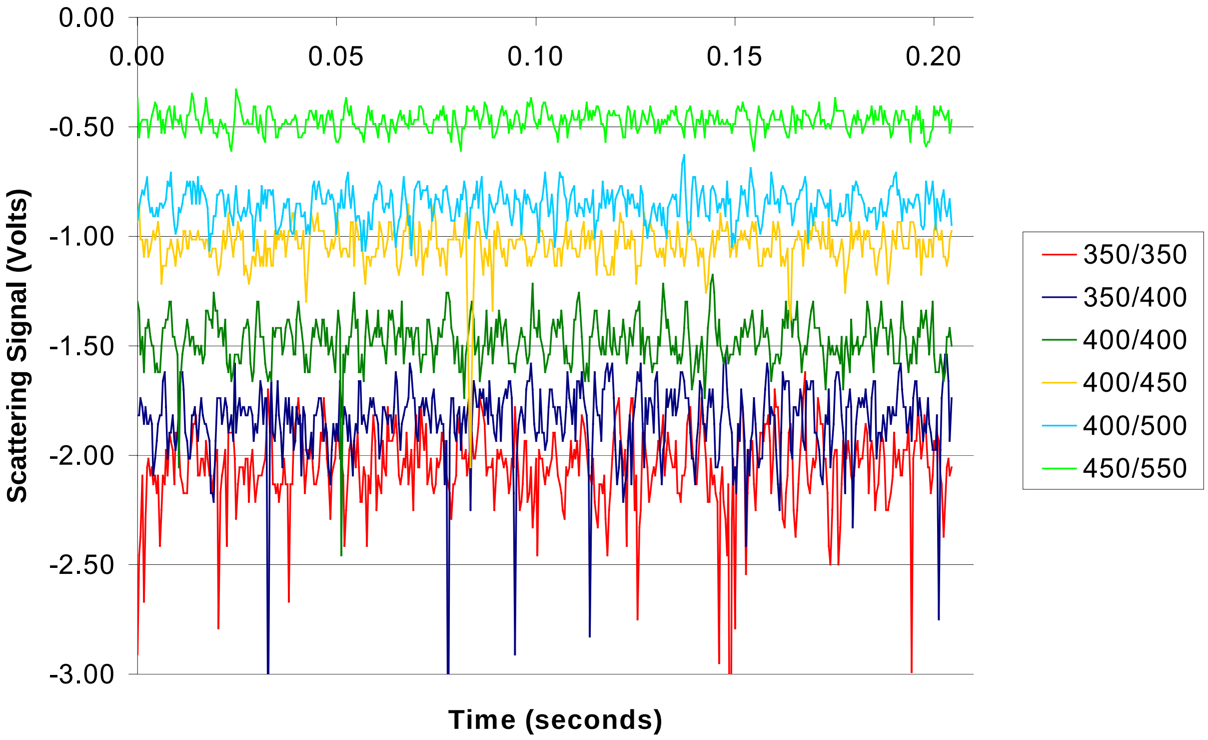

FIGURE 13: Time traces of scattering signal for 4.1/85/85 slpm stage air flow split, and fuel-air equivalence ratio of 0.5. The stage temperature split is given in the legend.

Figures 14 and 15 show the time traces for the atomizer air increased to 5 slpm and the second stage air maintained at the highest flow rate tested: 85 slpm. Runs with the first stage air reduced to 44 slpm, giving a 1st to 2nd stage air split of about 1:2 are plotted in Figure 14, and runs with the first stage air increased to 85 slpm are shown in Figure 15. With the atomizer air increased to 5 slpm, and with the first stage air decreased to provide more residence time in stage 1, the traces of Figure 14 show no evidence of droplet scattering. In Figure 15, with the first stage air increased to its highest flow rate tested, some indication of droplet scattering is in evidence. However, the droplet scattering is considerably reduced from the case of Figure 13. Clearly, the increase in the atomizer air flow rate reduces the amount of droplet material at the exit of the SPP.

Vapor lock was not experienced in the LRS experiments.

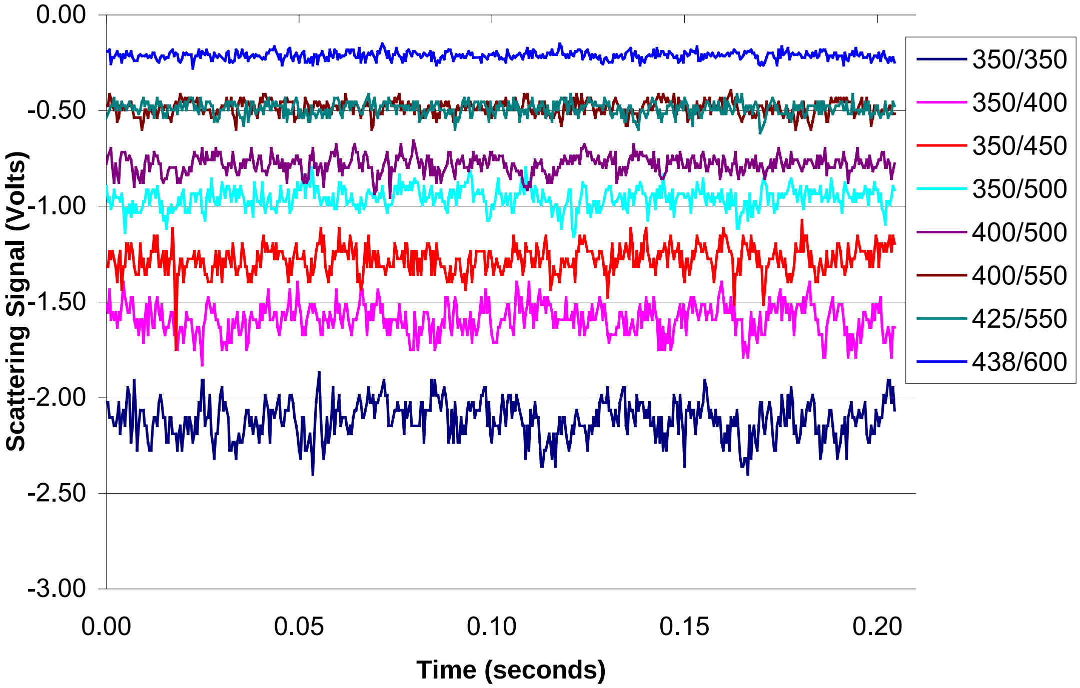

FIGURE 14: Time traces of scattering signal for 5/44/85 slpm stage air flow split, and fuel-air equivalence ratio of 0.5. The temperature split is given in the legend.

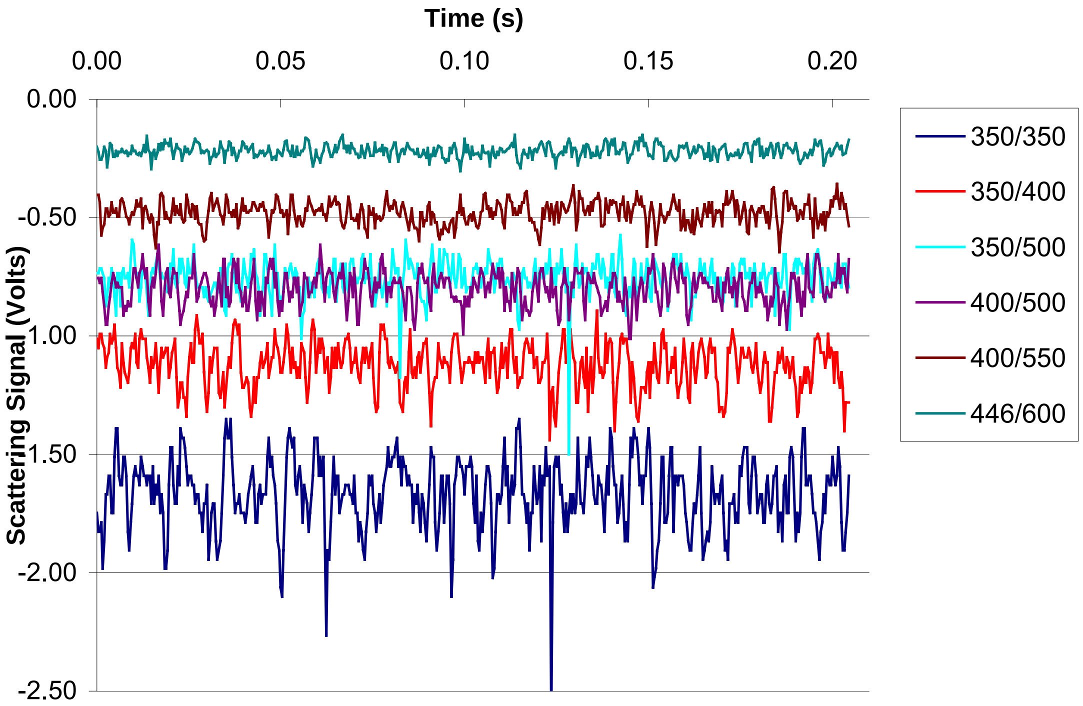

FIGURE 15: Time traces of scattering signal for 5/85/85 slpm stage air flow split, and fuel-air equivalence ratio of 0.5. The stage temperature split is given in the legend.

Figure 16 shows the time-mean scattering measurement for all of the LRS tests conducted with the 5 slpm atomizer air. The stage 2 temperature is used as the variable, since it is very close to the outlet temperature of the SPP.

The time-mean scattering deceases with increasing temperature and decreasing diesel fuel present. Although note shown in Figure 16, decreasing phi decreased the scattering signal. The decrease in scattering with increasing temperature seen in Figure 16 is expected based on Equations 4 and 5 above. However, the scattering falls off faster than 1/T(K) predicted by ideal gas theory. There are at least two possible explanations for this temperature behavior of the scattering signal:

- The behavior of the diesel vapor is more complex than predicted by ideal gas theory, especially at the lower temperatures.
- Cracking reactions produce lighter species that reduce the scattering at the higher temperatures.

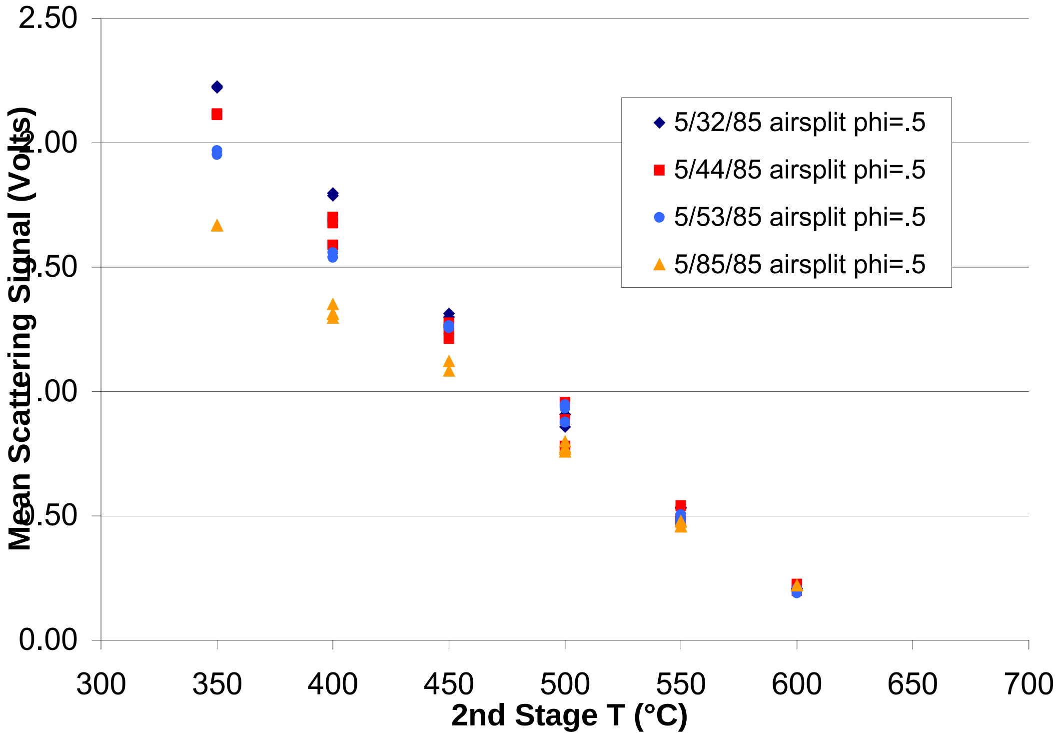

FIGURE 16: Mean scattering signal as a function of 2nd stage temperature.

Figures 17 and 18 show the ratio of the standard deviation over the time-mean of the scattering signal. This ratio is used as an indicator of unmixedness of the diesel fuel with the air. In Figure 17, the ratio is plotted against the SPP 1st stage temperature, and in Figure 18 the ratio is plotted against the 2nd stage temperature. The nominal baseline noise level of the system is also shown. This level corresponds to the inherent background noise of the system with the laser power set at its normal operating condition and with the detection and recording electronics set at sensitivities used to record about a 2 volt scattering signal. All of the data shown in these two figures are for an atomizer air flow rate of 5 slpm. Thus, the impact of scattering from droplets is fairly weak.

For most of the runs, the standard deviation over mean falls within the range of 0.05 to 0.10. Several of the runs are close to the background noise level of the diagnostic system, indicating mixedness close to complete.

Droplets in the SPP outlet increase the standard deviation over mean ratio. With the use of atomizer air in the range of 3.6-4.1 slpm, this effect was noticed for the data at the lowest temperatures. However, it is not much noticed in Figures 17 and 18, because of the use of the 5 splm atomizer air.

Figures 17 and 18 do show an increase in the standard deviation over mean at the highest temperatures. There are two possible explanations for this behavior:

1. With increasing temperature, the residence time within the SPP decreases, leaving less time to accomplish mixing of the fuel vapor with the air.
2. With increasing temperature, the scattering single decreases (see Figure 16), requiring an increase in the sensitivity of the electronic equipment. The increase in the signal noise caused by this change probably has the greatest effect of the standard deviation over mean.

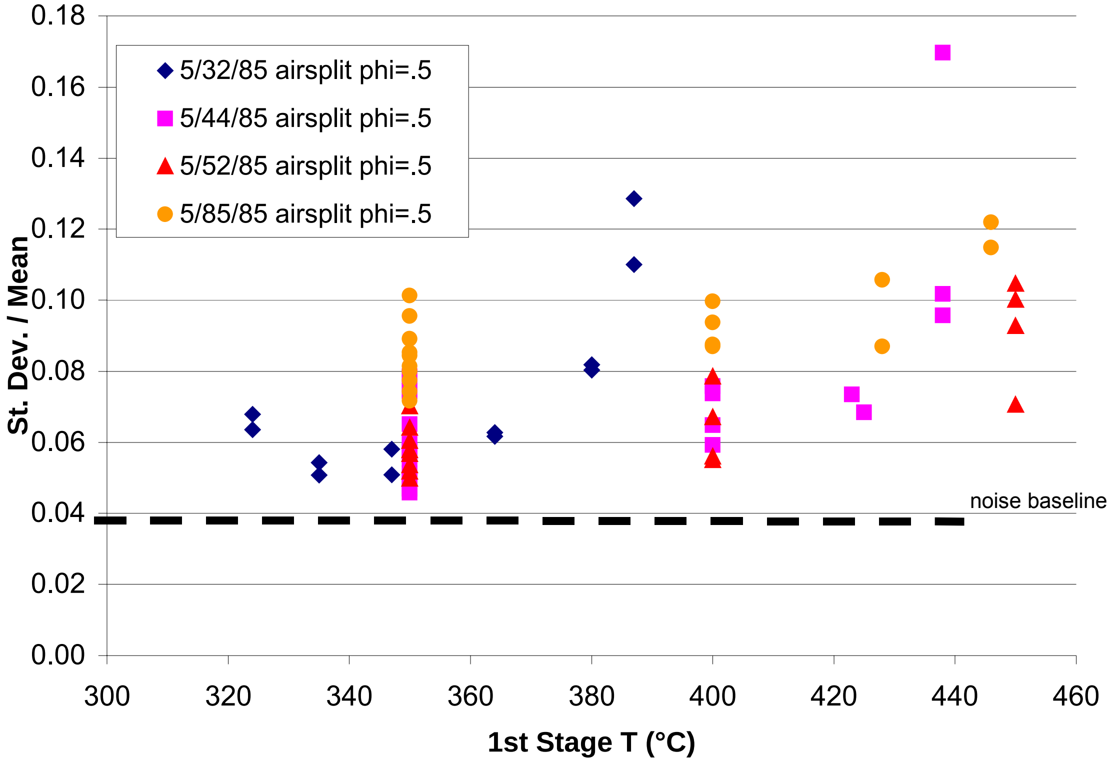

FIGURE 17: Standard deviation over time-mean ratio of scattering plotted as a function of 1st stage temperature.

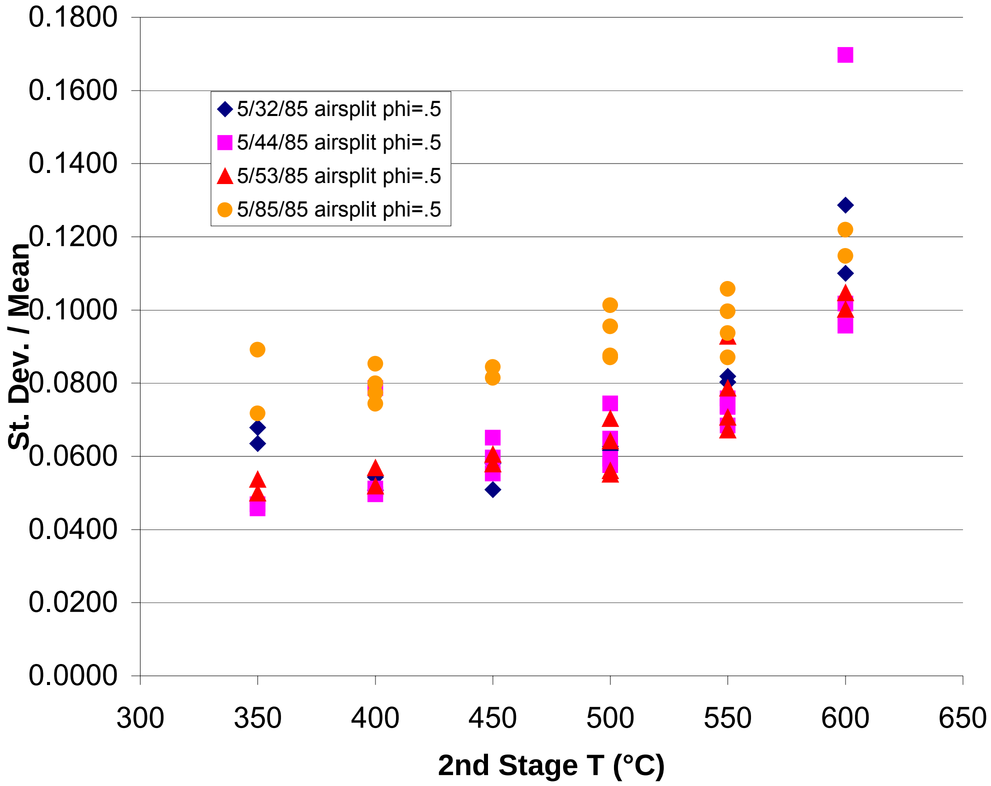

FIGURE 18: Standard deviation over time-mean ratio of scattering plotted as a function of 2nd stage temperature.

CFD MODELING OF THE LABORATORY SPP

Modeling of 2 atmosphere SPP operation at 12-16 ms residence time

The laboratory SPP has been modeled using a commercial CFD code. The velocity and temperature fields are found by a time-steady RANS simulation without diesel fuel injection. Then the diesel injection is modeled using Lagrangian particle (droplet) tracking. The injection point is modeled as an air-blast atomizer. More detailed on the CFD modeling is described below in the section entitled: CFD Modeling of the Industrial SPP.

Two cases were modeled, similar to cases from Table 7:

- Low temperature case: 250/350 degrees C temperature split, with overall SPP residence time of about 16 ms and fuel-air equivalence ratio of 0.55.
- High temperature case: 436/550 degrees C temperature split, with overall SPP residence time of about 12.5 ms and fuel-air equivalence ratio of 0.49.

For both cases, the pressure within the SPP was about 2 atm (absolute), and the air flow split was 50/100 slpm.

Table 11 gives the conditions input to the CFD modeled. The temperatures have been adjusted to the stage 1 and 2 air inlet temperatures, and the stage 1 air includes the 5 slpm of atomizer air.

Table 11: Conditions for CFD modeling of laboratory SPP

	Cool case (1)	Hot case (2)
Pressure, atm	1.978	2.05
phi	0.55	0.49
1st stage air flow, kg/s	1.1e-3	1.1e-3
1st air inlet temperature, K	588	773
2nd stage air flow, kg/s	2e-3	2e-3
2nd stage air inlet temperature, K	673	873
Fuel flow rate kg/s	1.051e-4	9.087e-5

The results of the CFD modeling are presented by the figures that follow.

The velocity and the temperature profiles are very similar in both cases. The highest velocity is in both cases near the secondary stage air inlet. Figure 19 shows the velocity magnitude for the hot case. The outlet velocity is relative low (about 15 m/s). This is consistent with the relative long residence time of 16 ms.

Figures 20 and 21 show the temperature fields for the two cases.

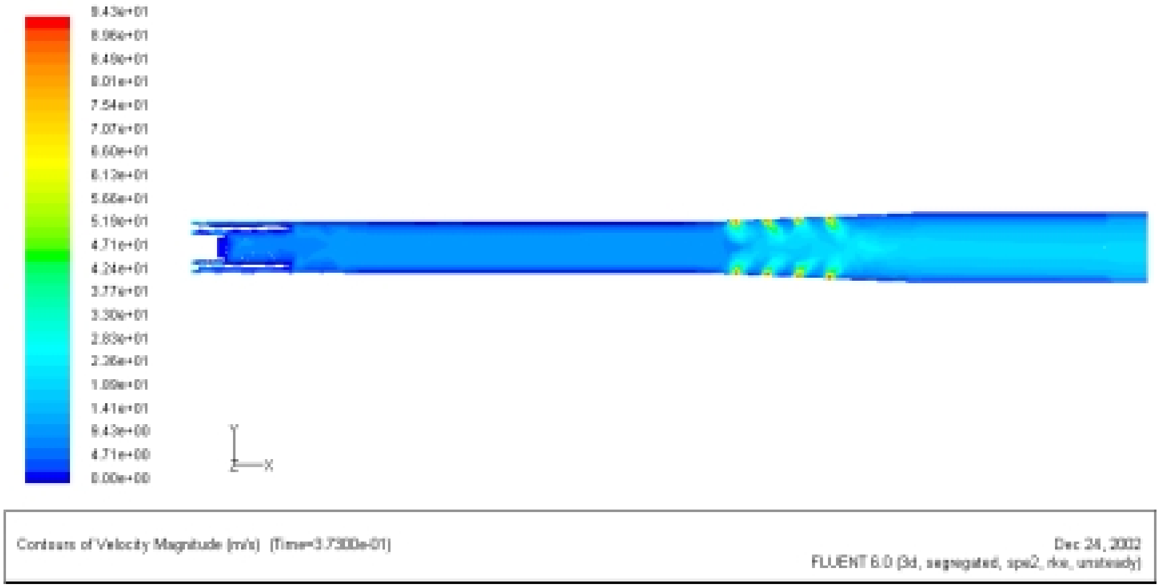

Figure 19: Velocity magnitude for the hot case – maximum velocity is 94 m/s and average axial velocity at the exit plane is about 15 m/s.

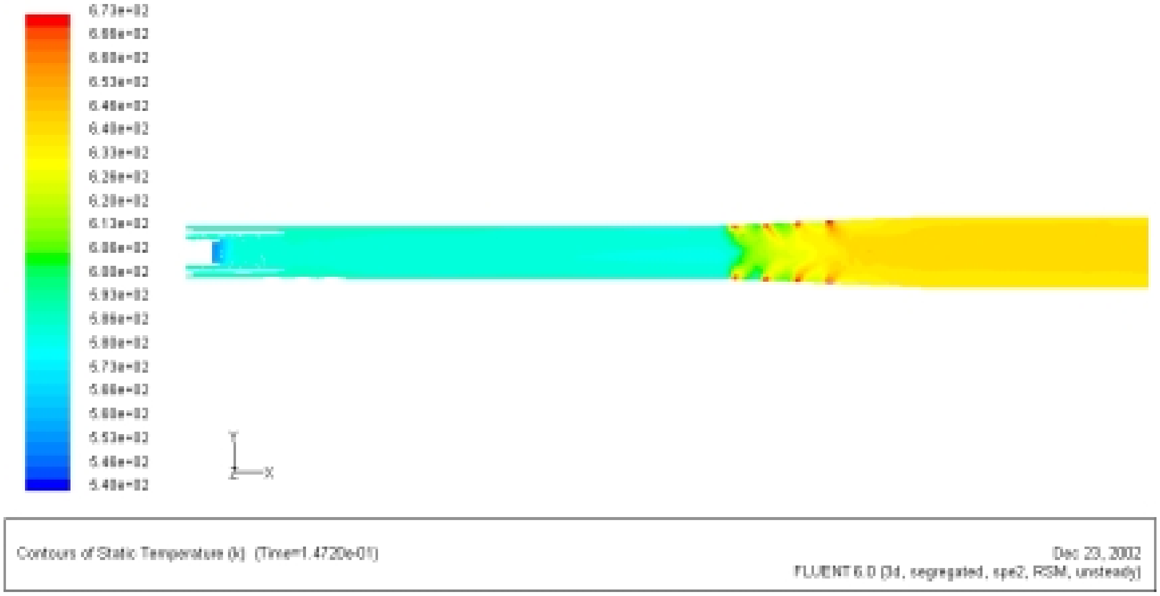

Figure 20: Static temperature for the cool case – average exit plane temperature of 641 K (368 degrees C).

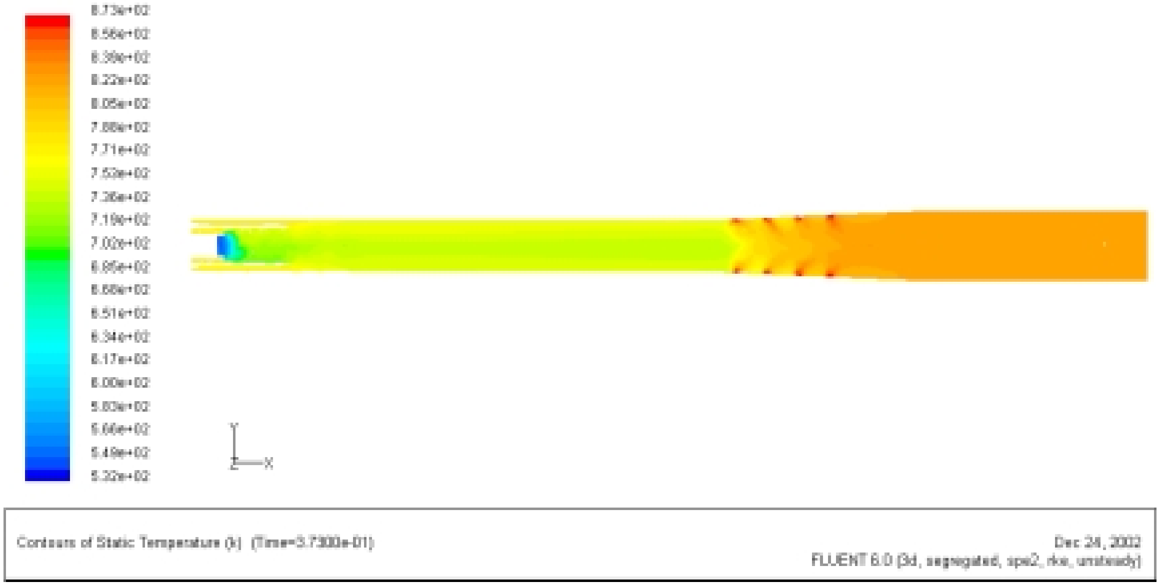

Figure 21: Static temperature for the hot case – average exit plane temperature of 828 K (555 degrees C).

The minimum temperature in both cases is in the recirculation zone near the fuel nozzle at the upstream (left) end of the injector. There the fuel droplets become caught in the zone, evaporate and reduce the temperature.

Figure 22, below, shows the diesel vapor mole fraction for the hot case. The maximum mole fraction of the diesel vapor is about 2E-2. This occurs by droplet evaporation in the recirculation zone near the fuel nozzle point.

Figure 23 shows the exit plane distribution of the diesel vapor mole fraction for the hot case. The diesel vapor fraction varies about ±10% about the mean value.

Figures 24 and 25 show diesel particle (droplet) tracking for the two cases. Key points are as follows:

- Figure 24: cool case: there are number of particles leaving the domain through the SPP outlet not evaporated. Maximum temperature of the droplets is 484 K at the outlet plane.

- Figure 25: hot case: there are no particles leaving the domain through the SPP outlet not evaporated. Maximum temperature of the droplets is 493 K. Some of the droplets get caught in the recirculation zone at the injector and evaporate in that region.

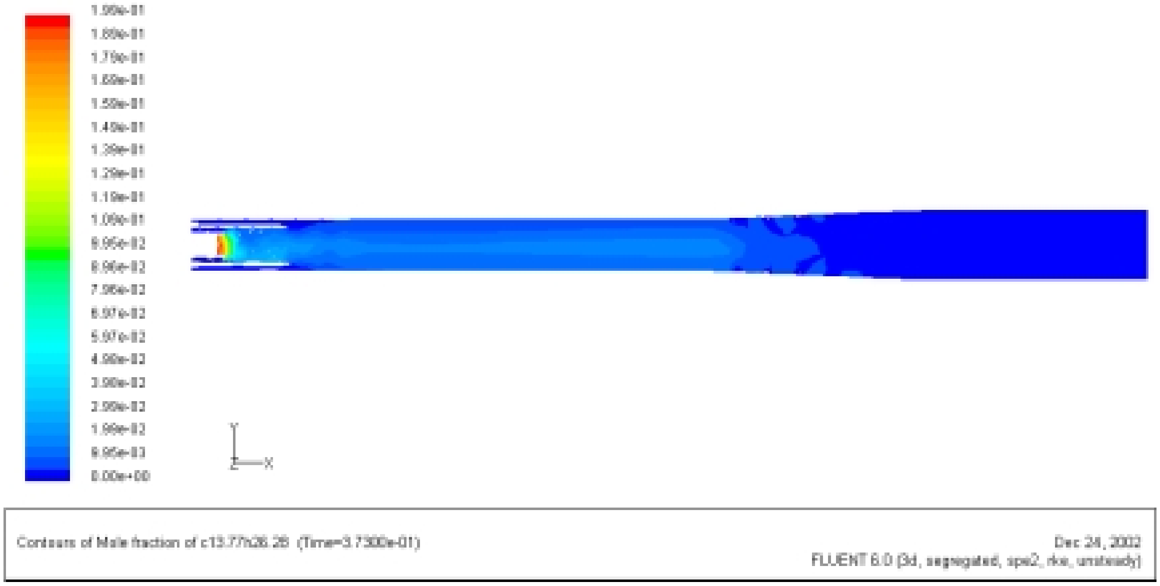

Figure 22: Mole fraction of vaporized diesel fuel for the hot case.

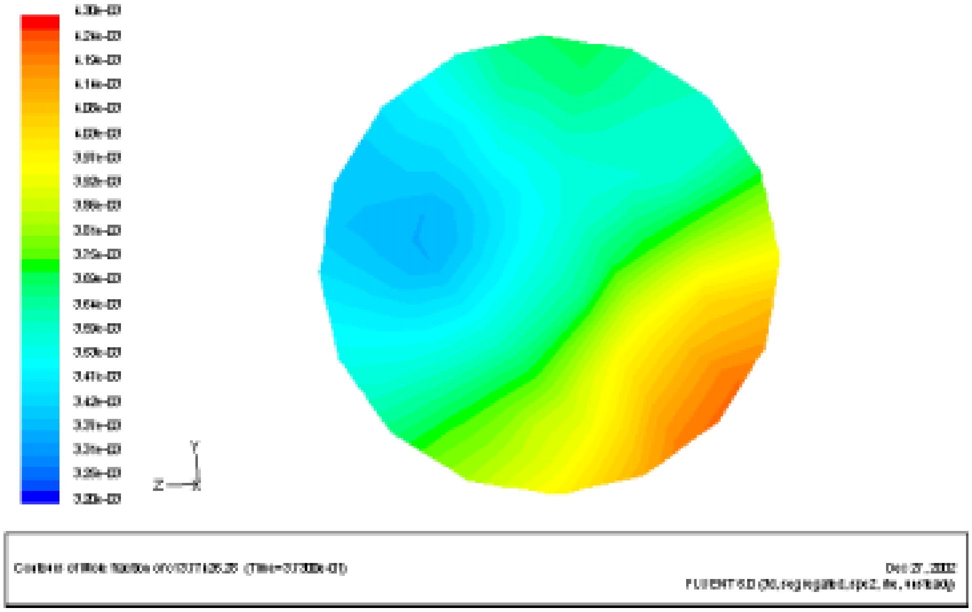

Figure 23: Mole fraction of evaporated fuel at the outlet -- the mean value is 0.00368 mole fuel/ mole total.

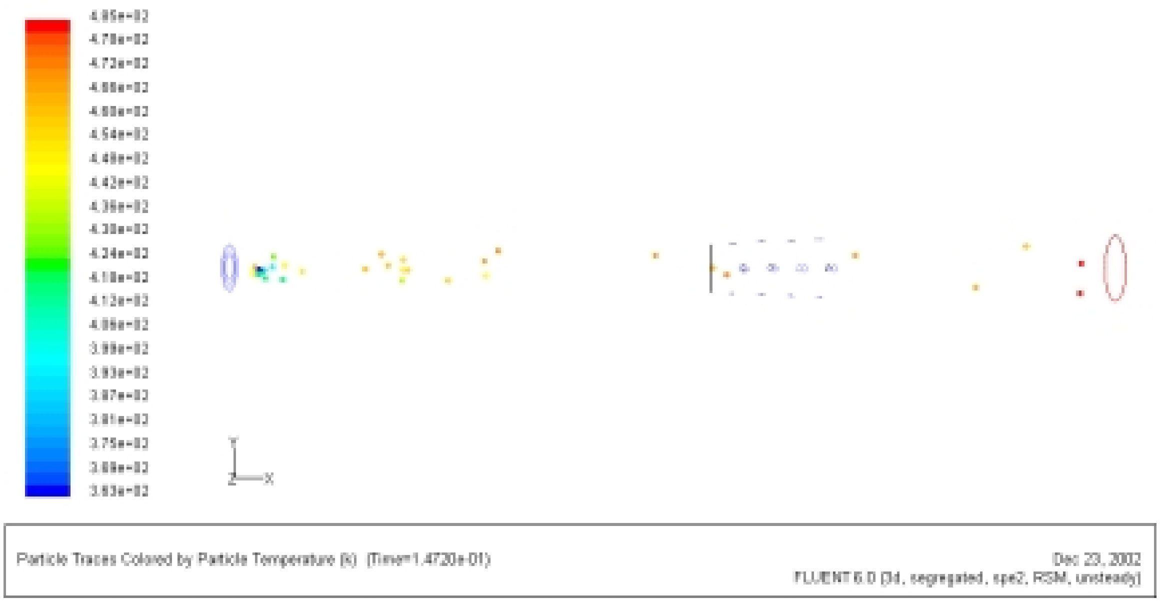

Figure 24: Diesel particle traces colored by droplet temperature for the cool case.

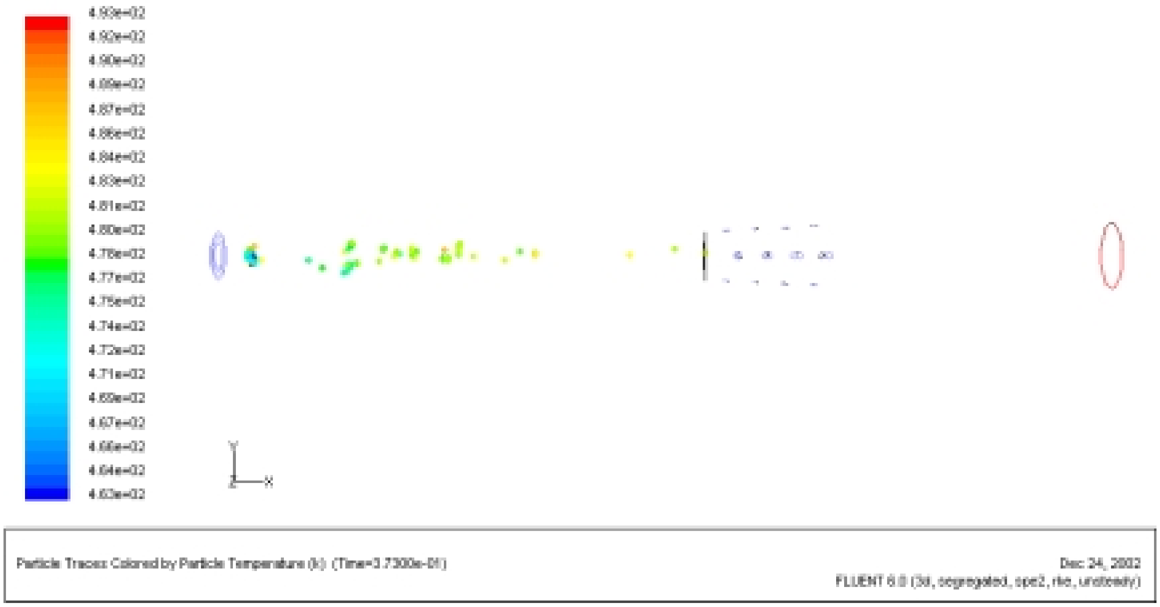

Figure 25: Diesel particle traces colored by droplet temperature for the hot case.

Modeling of 30 atmosphere SPP operation at 5-6 ms residence time

Figure 26 show results from CFD modeling of the laboratory SPP operated at 30 atmosphere pressure and high velocity, leading to a residence time of 5.8 ms. From top to bottom in this figure, the SPP is illustrated by gas temperature, fuel vapor mass fraction, and gas velocity magnitude. The flow is from left to right. At the left (upstream) end of the SPP, the stage 1 air enters as streams on both sides of an annular air flow splitter. The No. 2 diesel fuel spray enters at the upstream end, dispersed as a cone around the centerline. Initial fuel droplet size is 15 μm. At stage 2 (right 40% of the figure), air enters through 45° radial jets. The outlet pressure is 30 atm, and the pressure drop between the air inlet manifolds and the SPP outlet is 5%. The flow conditions in stages 1 and 2 of the SPP are given in Table 12. The pressure is 30 atm (at the SPP outlet) and the 2nd stage air inlet temperature is 823 K. The residence time in the 2nd stage is reduced to 1.63 ms by increasing the mass flow rate of the SPP. In order to maintain the overall air pressure loss of the SPP at 5%, the 2nd stage air inlet jets are increased in size (each of the 16 jets is given a diameter of about 1 mm). For the exit plane of the SPP, the CFD solution of the Reynolds averaged Navier Stokes equations gives a fairly small spatial variation in the fuel vapor mass fraction, indicated by a standard deviation over mean value of about 0.08. Because of the injection of the 2nd stage air towards the centerline of the SPP, slightly reduced levels of fuel vapor are seen in the center of the exit plane.

Table 12: SPP conditions for pressure of 30 atm.

Value	Stage 1	Stage 2
Temperature of inlet air, °C (K)	473 (746)	550 (823)
Mass flow rate within SPP, kg/s	0.061	0.184
Residence time within SPP, ms	4.16	1.63

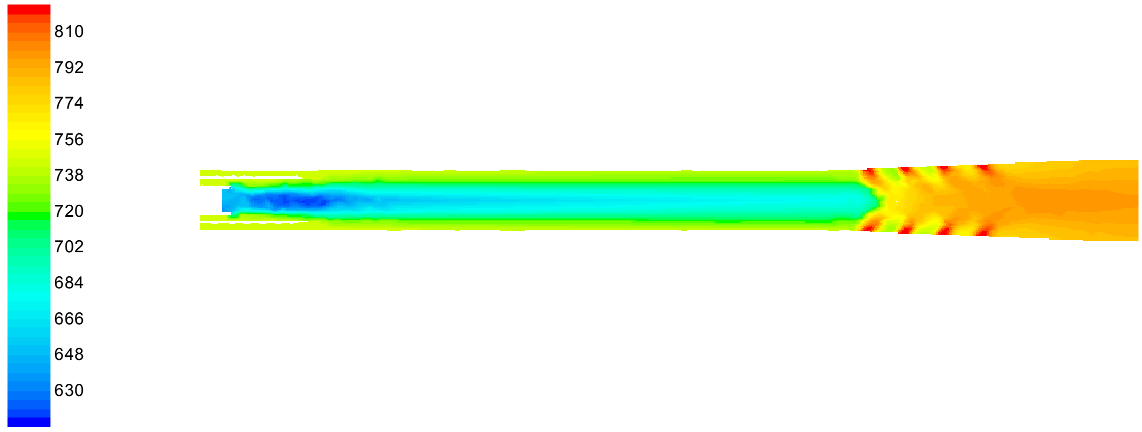

Gas Temperature (K)

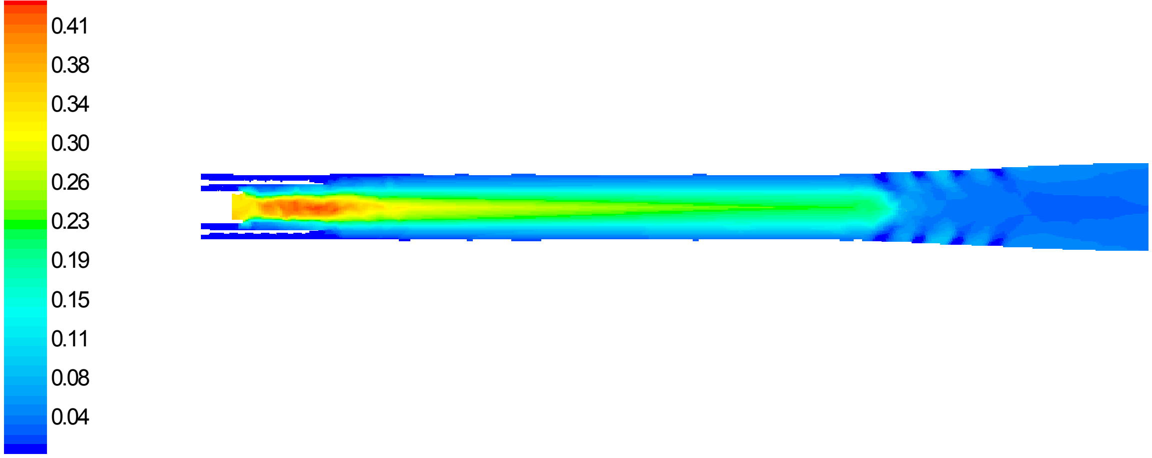

Fuel Vapor Mass Fraction

Gas Velocity Magnitude (m/s)

Figure 26: CFD simulation of 30 atm operation of the laboratory-scale SPP

INDUSTRIAL SPP

This section was provided by the Gas Turbine Fuel System Division of the Parker Hannifin Corporation. The design and fabrication of the industrial SPP was conducted by Parker Hannifin Corporation.

> "Parker has retrofitted the Parker premixer to achieve the requirements of the SPP. The airflow is now staged to allow two air inlets at two different temperatures. A plenum surrounding the axial flow at the base of the premixer was designed to allow for stage 1 air feed. Stage 2 air enters the premixer through the radial in flow swirler.
>
> The larger flange that mounts to the combustor was also built and shipped to Solar Turbines for the combustion tests. The fuel injection unit was also redesigned and reconditioned for these tests.
>
> The following images show the details of the setup."

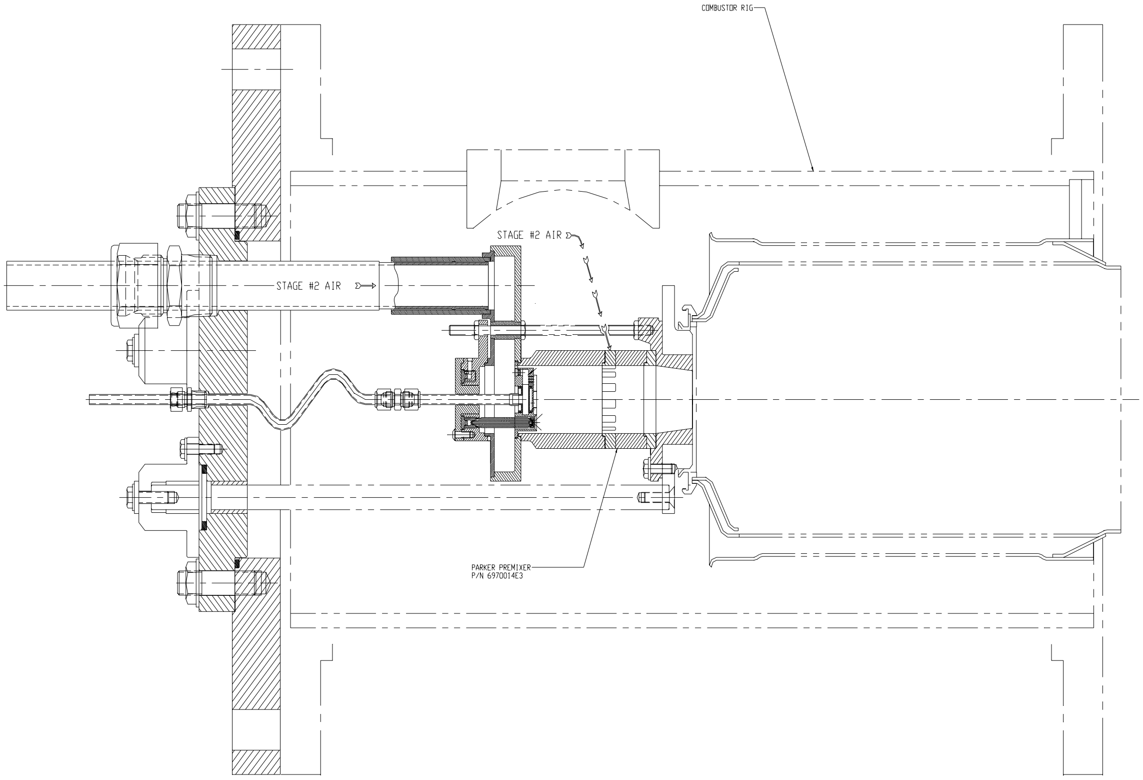

Figure 27: Industrial SPP with housing and combustor (provided by Parker Hannifin Corporation).

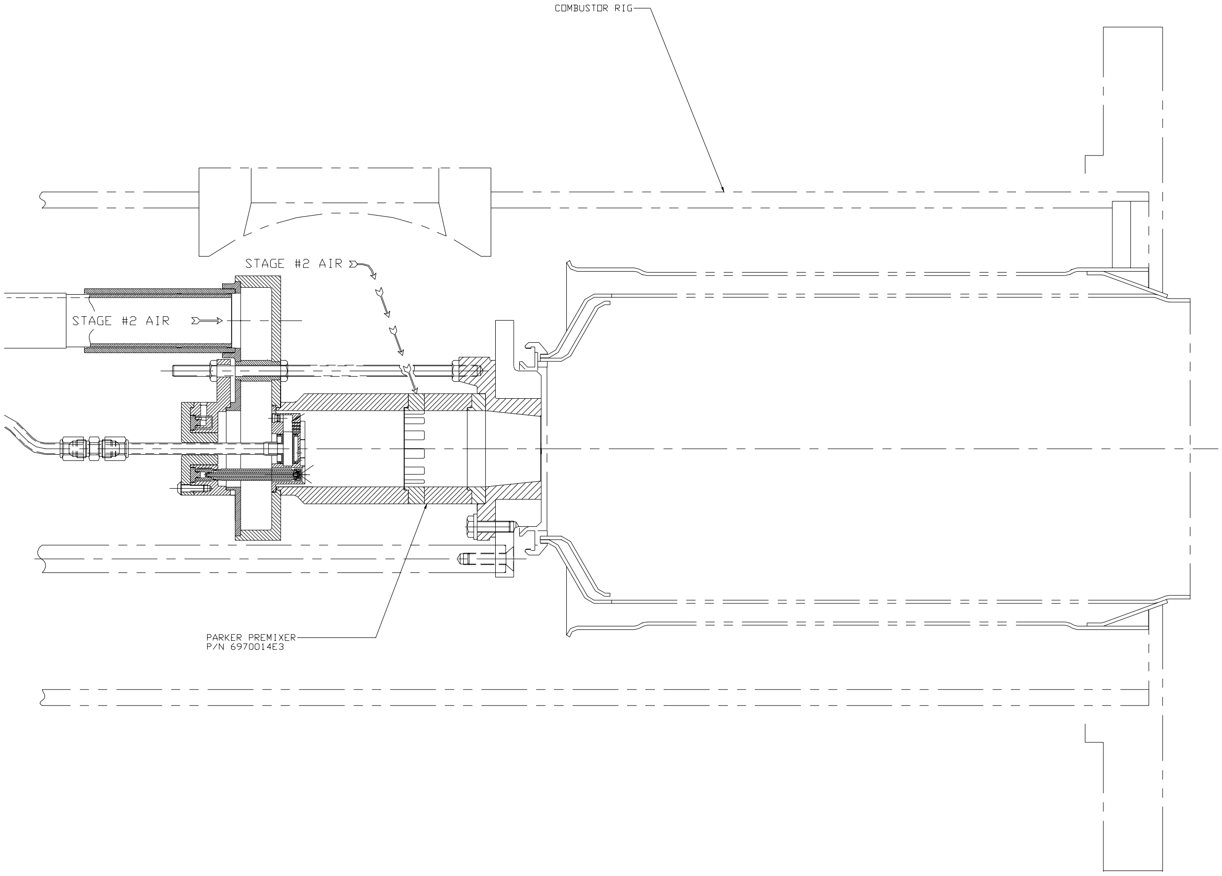

Figure 28: Industrial SPP with combustor (provided by Parker Hannifin Corporation).

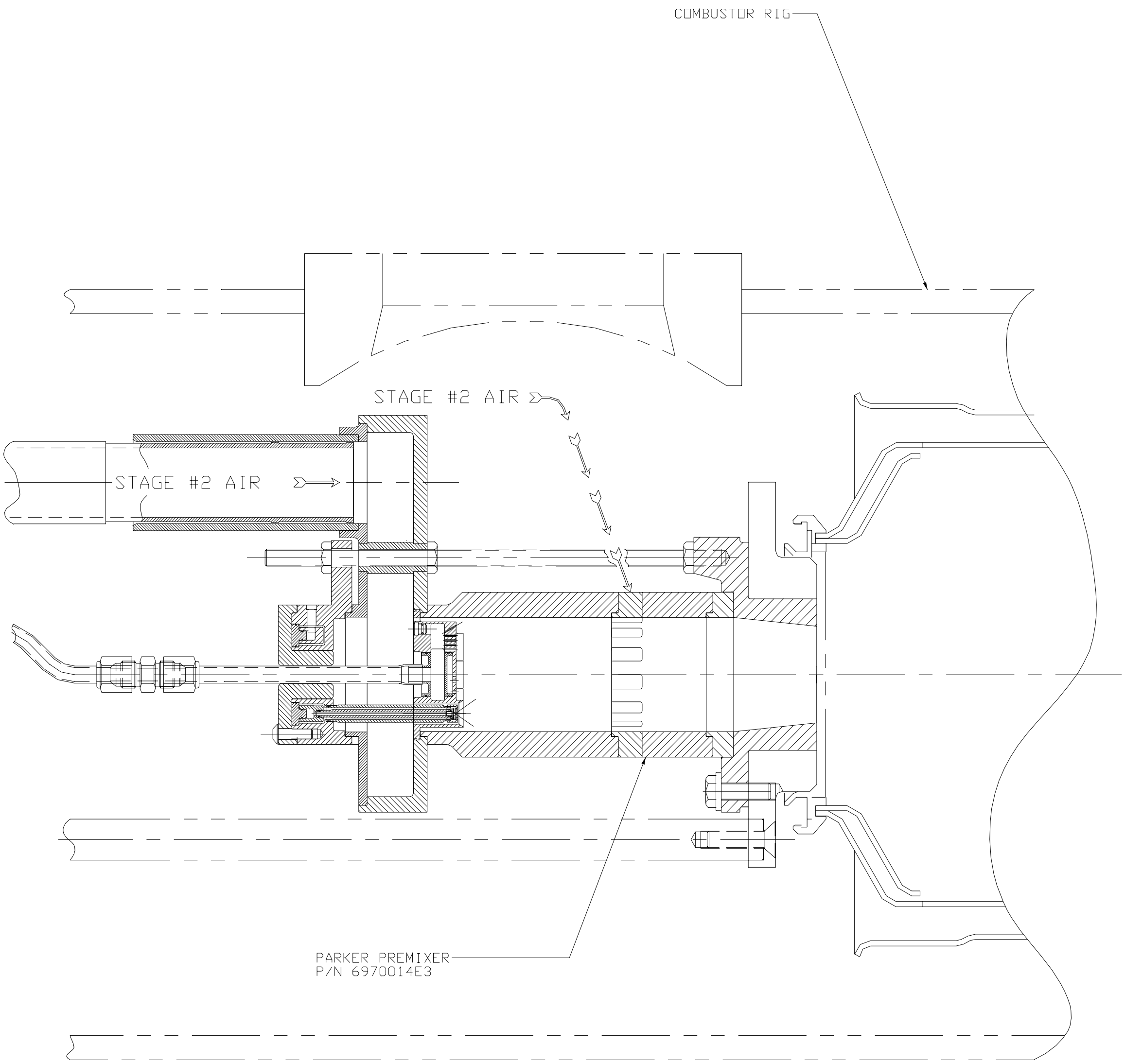

Figure 29: Industrial SPP (provided by Parker Hannifin Corporation).

DEVELOPING THE TEST SETUP FOR THE INDUSTIAL CELL

Testing of the industrial SPP is scheduled for Solar Turbines, Inc.

Photographs of the test cell at Solar Turbines modified for testing of industrial SPP are shown in Figures 30-34.

- Figure 30 shows the piping and metering valve installed for the SPP testing.
- Figure 31 shows the piping from a different angle.
- Figure 32 shows the orifice meter installed for the SPP testing.
- Figure 33 shows the test rig originally proposed for the SPP testing.
- Figure 34 shows new test rig scheduled to be used for the SPP testing.

The rig is designed so that the industrial can be tested for pressures of 10-16 atm and for 2nd stage inlet air temperature up to about 600 degrees C.

The status of the testing of the industrial SPP is indicated in following correspondence received from Solar Turbines, Inc.

August 2002:

> "Solar is pleased to be working with the University of Washington (UW) in the DOE-supported evaluation of the high-pressure staged prevaporizer-premixer (SPP). At this point nearly all the necessary modifications to the test facility at Solar have been completed.
>
> Progress on specific tasks is detailed below:
>
> - The injector modification has been completed by Parker Hannifin Corporation.
> - The first stage hot air regulator valve has been upgraded and installed
> - The required shut-off valve has been purchased but needs to be installed
> - Plumbing has been purchased, installed and inspected
> - The flow metering orifice plate has been purchased and installed

We apologize for the delay in testing that has occurred. The delay has been the result of:

- Scheduled air system maintenance and improvements took longer than planned
- A series of production-related issues
- Most recently the need to replace the test rig itself because of cracks found in the pressure vessel.

Currently, we are in the process of installing a new test rig. There will be some time required for rig “shake-down”.

We understand the urgency of the SPP testing for both UW and the program sponsors. Solar will make every effort to complete the high pressure evaluation as soon as possible. We appreciate your patience as we work through the problems that have caused the delay of these tests.”

November 2002:

“There has been some unforeseen, but somewhat expected, delays in the UW SPP testing at Solar.

We ran into some rig "issues" upon commissioning (the new rig) and these issues have caused several delays. Currently, we are forecasting to complete the SPP testing shortly after (holiday) break during which we can complete the upgrades and modifications for SPP testing.

We believe and would very much like to complete the SPP testing by the end of the first quarter, 2003.”

Figure 30: SPP 1st stage air metering valve (photo provided by Solar Turbines)

Figure 31: High pressure hot air diverted from Building 30, Cell 5 to Cell 6 (photo provided by Solar Turbines)

Figure 32: Orifice meter
(photo provided by Solar Turbines)

Figure 33: Originally proposed Cell 6 high pressure, single injector test rig.
(photo provided by Solar Turbines)

Figure 34: Newly constructed Cell 6 high pressure, single injector test rig. (photo provided by Solar Turbines)

CFD MODELING OF THE INDUSTRIAL SPP

In this section we use CFD to analyze the industrial SPP that was developed by Parker Hannifin Corporation using the “macrolamination” fuel atomization technology. This technology allows multi-point fuel injection, which has advantages over the single point injectors. This can lead to a reduced mixing time scale, and thus can reduce the tendency for auto-ignition and flashback.

The design of the injector prototype includes a row of in-flow swirlers and eight macrolaminate fuel injectors. The quarter sector of this SPP is shown on Figure 35. The air comes into the SPP at several locations. These locations were chosen to maximize the mixing rate and minimize the fuel accumulation on the wall. See Figure 36.

The first stage air enters this SPP at three locations:

1. Air enters around the macrolaminate injector tips assisting in accelerating the fuel droplets and atomizing the fuel.
2. Air enters the SPP along the outer wall. This prevents for the fuel droplets from hitting the wall and provides additional momentum to delay the boundary layer separation.
3. Air also enters axially through the series of holes located on the centerline. This pilot airflow prevents a large recirculation zone from forming on the centerline of the SPP.

The second stage air enters through the radial swirlers, which provide sufficient swirl for flame stabilization and help to keep the liquid fuel away from the wall.

The industrial SPP has been modeled using a commercial CFD code. The grid for the model was developed by Parker-Hannifin Corporation and consists of approximately 7E+5 tetrahedral cells. However, after the initial runs, we refined the grid to 1.5E+5 cells.

The CFD simulations were performed on the 64 processor parallel computer in the Mechanical Engineering Department of the University of Washington. In the CFD simulation the code solves the Reynolds averaged Navier-Stoke Equations (RANS) using a finite difference scheme. The moment equations are closed using the seven-equation Reynolds Stress Model (RSM). This model was chosen due to the strong swirl and inherent non-isotropy of the flow and the stresses. In this study, the second order simulation did not converge so the present results show the first order RSM computation. First, the air flow is modeled as a steady-state problem without droplets. When the steady state solution was obtained, the second order unsteady implicit calculations were performed to predict the behavior of individual droplets in the SPP. Several discrete-phase models were used in the unsteady calculations of the droplet behavior, including droplet collision and interaction with the mean flow.

The boundary conditions were dictated by the operating conditions of the gas turbine engine.

Boundary conditions:

- First stage air at 650K, flow rate is 0.11kg/s.
- Second stage air at 800K and assigned pressure drop of 8% to achieve 50/50 distribution by mass of primary and secondary air flow rates.
- The mass flow rates were assigned to match the target axial outlet velocity of 50 m/s.
- Outlet pressure was assigned as 16 atm.

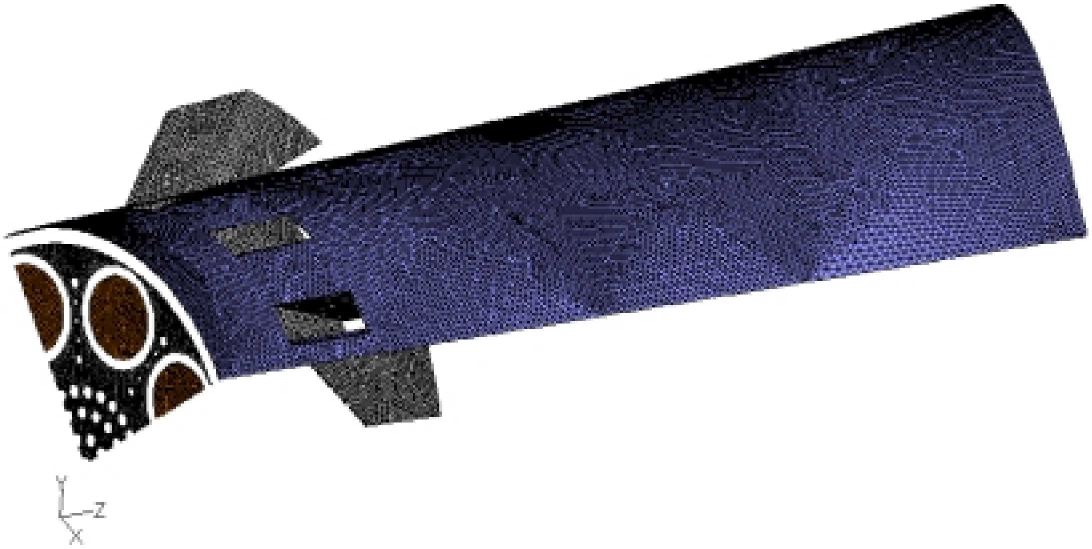

Figure 35: Industrial SPP, general layout

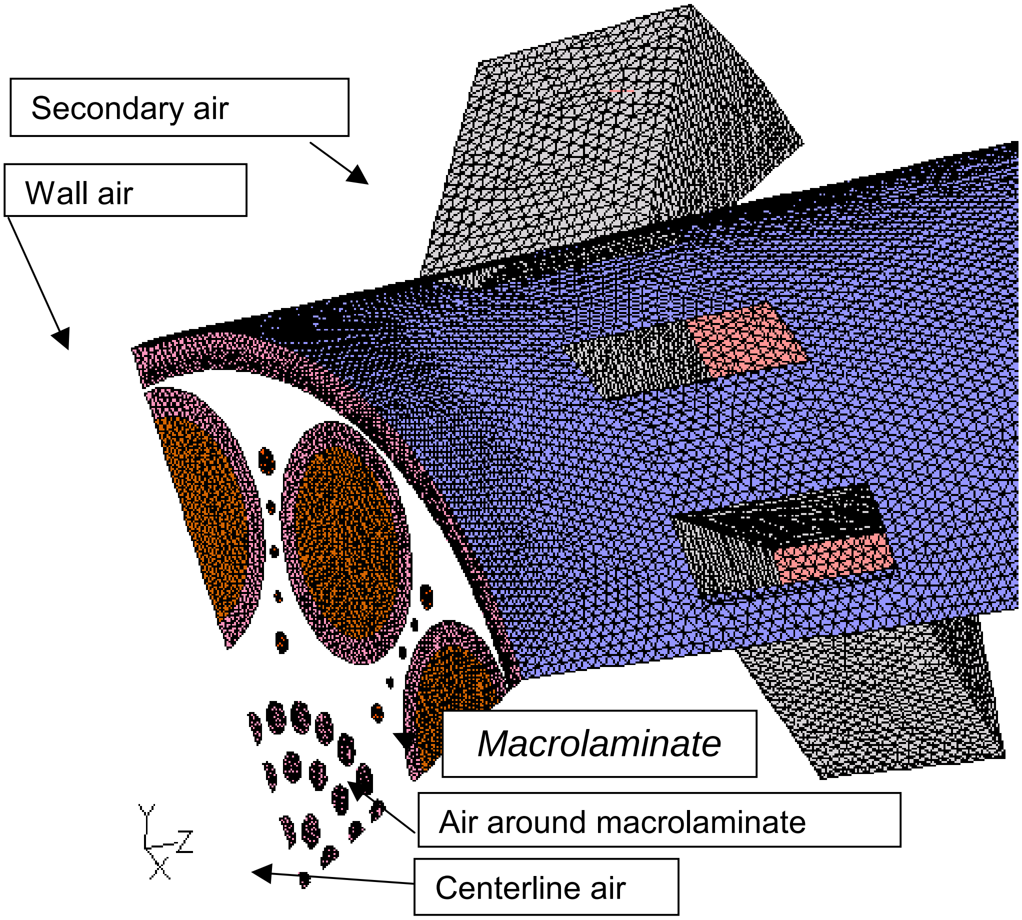

Figure 36: Close view of air inlets

Results of the unsteady RSM simulation: Figures 37 and 38 depict the particle (droplet) positions at a time of 0.05 ms after the initial injection. The injection is setup as a cone with appropriate velocity and spray angle. Figures 39 shows the particle positions colored by their diameter 3.6 ms after the start of the simulation, and Figure 40 after 5ms. In this run with the initial and boundary conditions described above all the droplets evaporated before they reached the exit plane of the SPP.

Figures 41 through 42 are the velocity contour plots of different components on the y-z plane of the injector. The maximum velocity is observed in the region where the 2nd stage air merges the 1st stage air jets. The pressure drop in this region is 7.5E+4 Pa which is about 4.5% of the operating pressure. See Figures 43 and 44.

Target axial velocity at the exit is 50 m/s. This velocity was achieved by assigning the pressure inlet boundary condition with 8% excess pressure for the 2nd stage air stream. The high pressure drop of the 2nd stage air can be explained (at least in part) by the high swirl number inside of the SPP.

In the simulation the majority of the second stage air does not penetrate to the center-line of the SPP, rather it creates the tangential flow used for the flame stability of the combustor. Thus the temperature profile at the exit plane is stratified (Figure 45). This effect is amplified by the droplet evaporation, which tends to cool the centerline flow. Minimum temperature at the exit is 550 K and the maximum is about 750K. The stratification of the flow can also be noticed on the contour plot of the fuel vapor mass fraction, where fuel tends to concentrate near the center-line making that zone effectively richer – see Figure 46.

Figures 47 through 49 show the velocity vectors colored by temperature and fuel mass fraction.

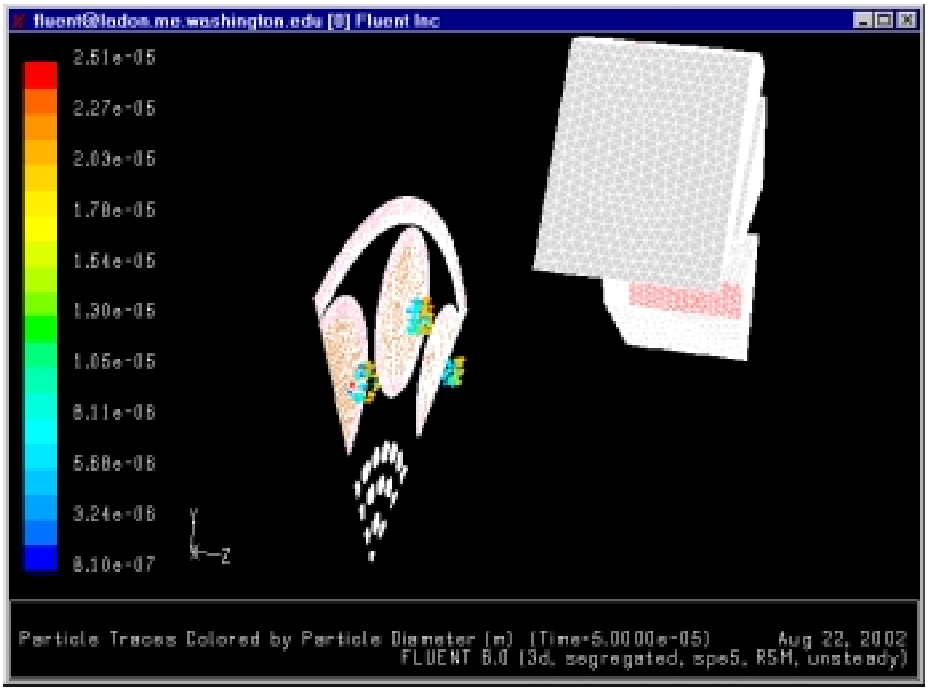

```
Particle Traces Colored by Particle Diameter (m)  (Time=5.0000e-05)       Aug 22, 2002
                                  FLUENT 6.0 (3d, segregated, spe5, RSM, unsteady)
```

Figure 37: Fuel droplets at time 5E-5 s. Note the coalescence of the droplets. The initial size is 20E-6m, the maximum size is 25E-6m.

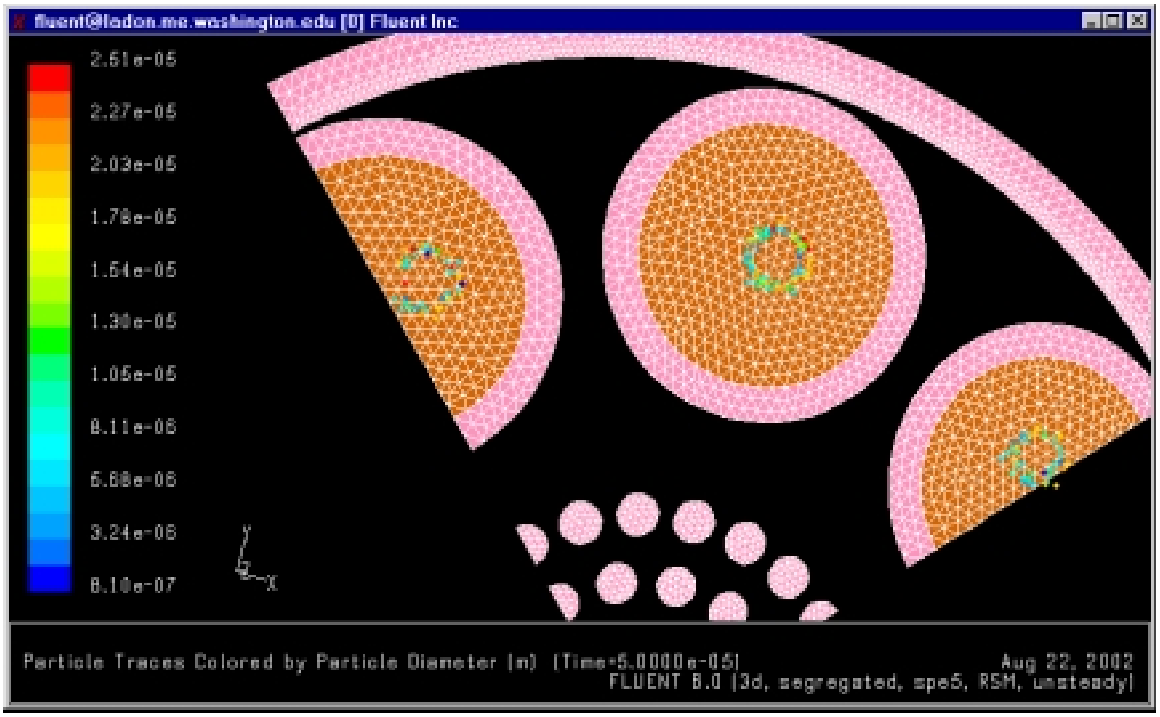

```
Particle Traces Colored by Particle Diameter (m)  (Time=5.0000e-05)                Aug 22, 2002
                                        FLUENT 6.0 (3d, segregated, spe5, RSM, unsteady)
```

Figure 38: Alternative view of Figure 37

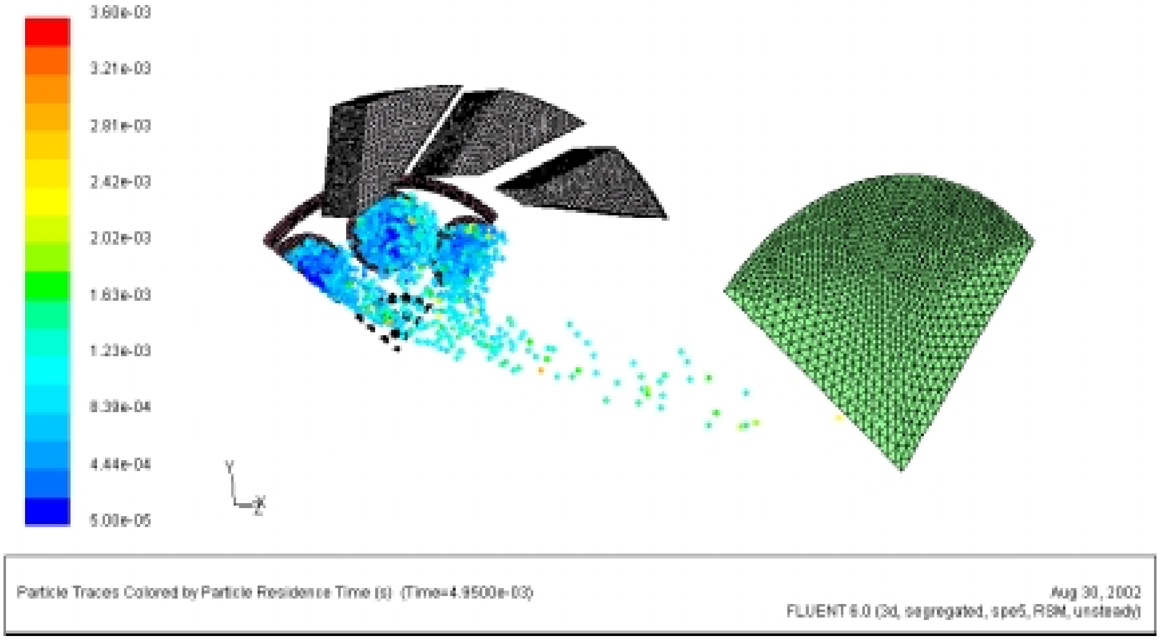

Figure 39: Fuel droplets colored by residence time, maximum residence time is 3.6 ms

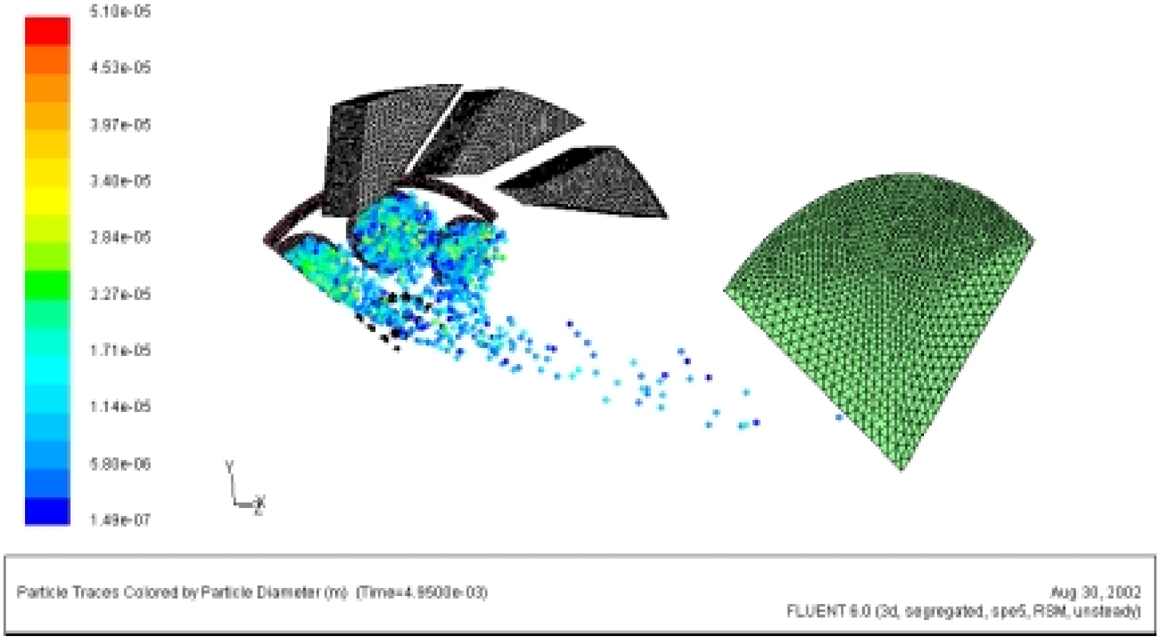

Figure 40: Fuel droplets colored by diameter, maximum droplet size is 51E-6 m, initial droplet size 20E-6m.

The pictures after 5ms from the initial injection

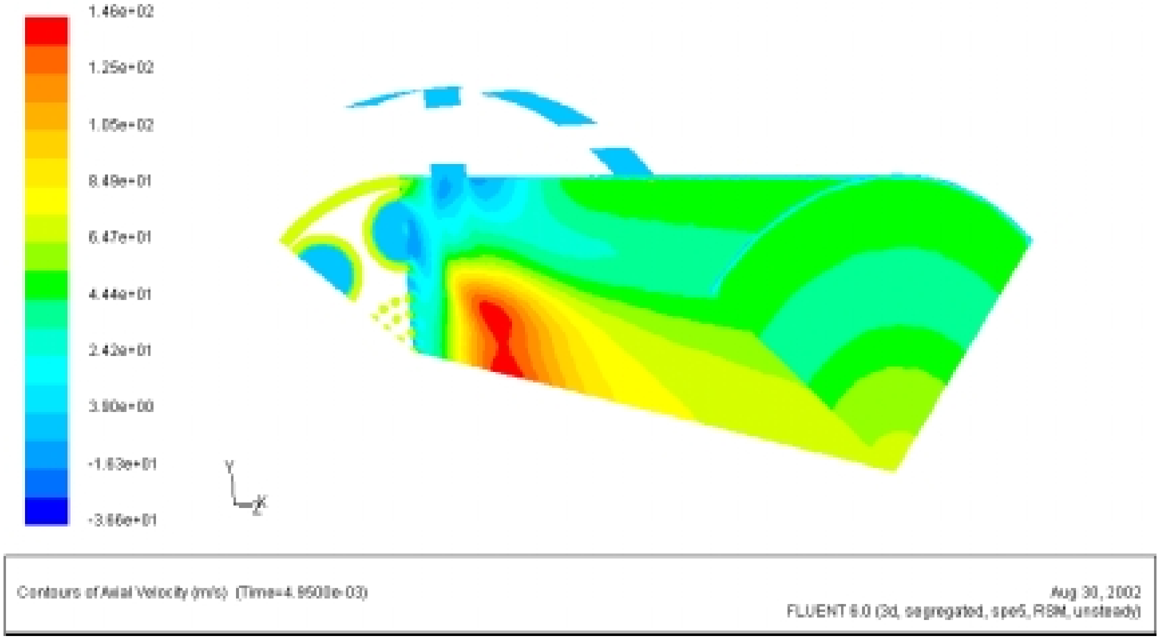

Figure 41: Axial velocity, outlet axial velocity component is 48m/s

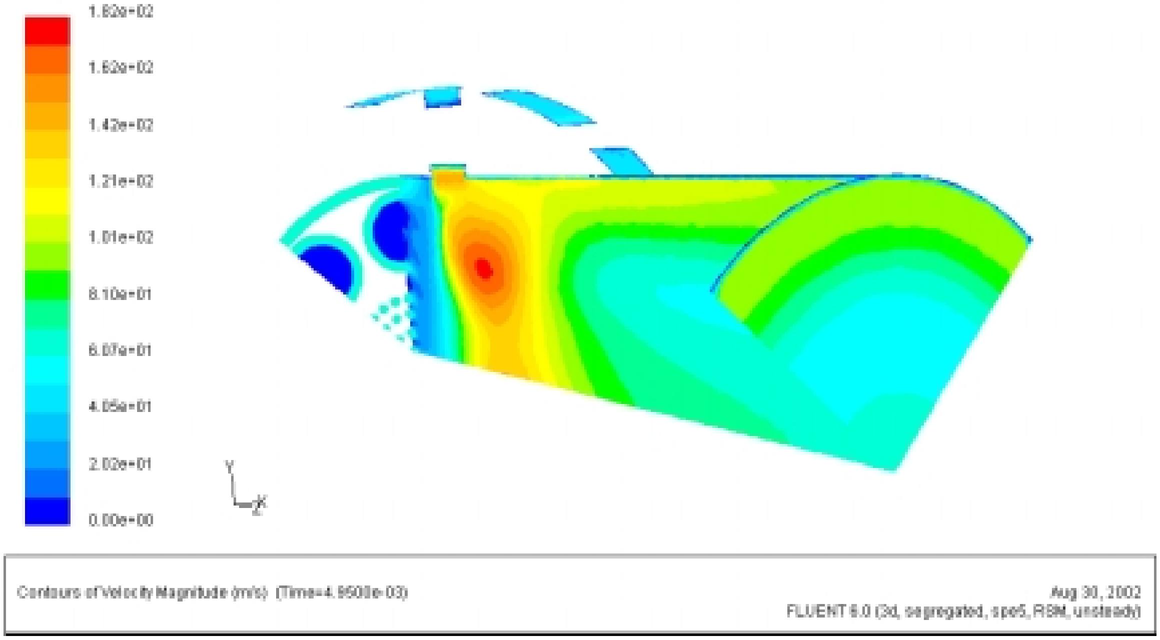

Figure 42: Velocity magnitude

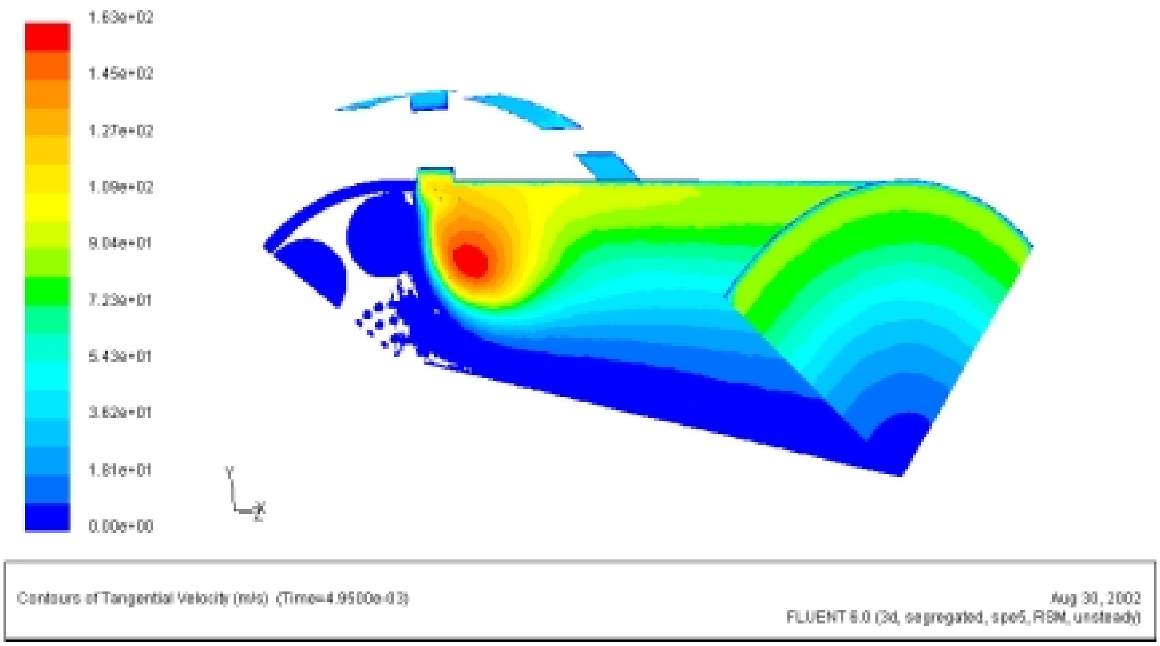

Figure 43: Tangential velocity component

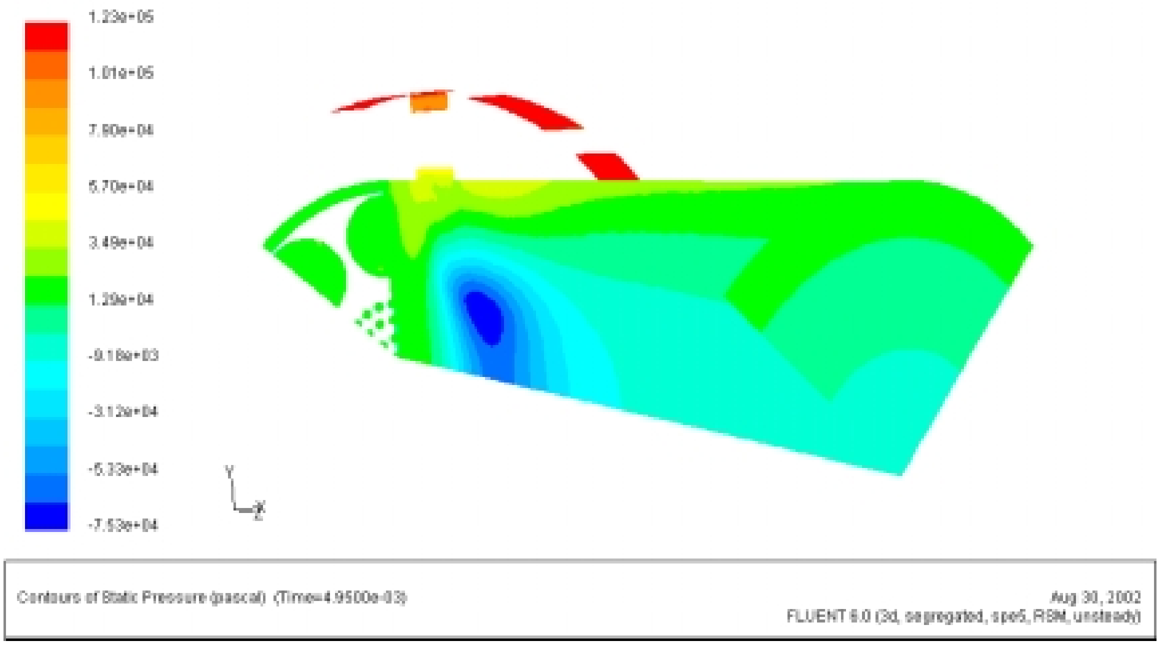

Figure 44: Static pressure, reference pressure is 16 atm.

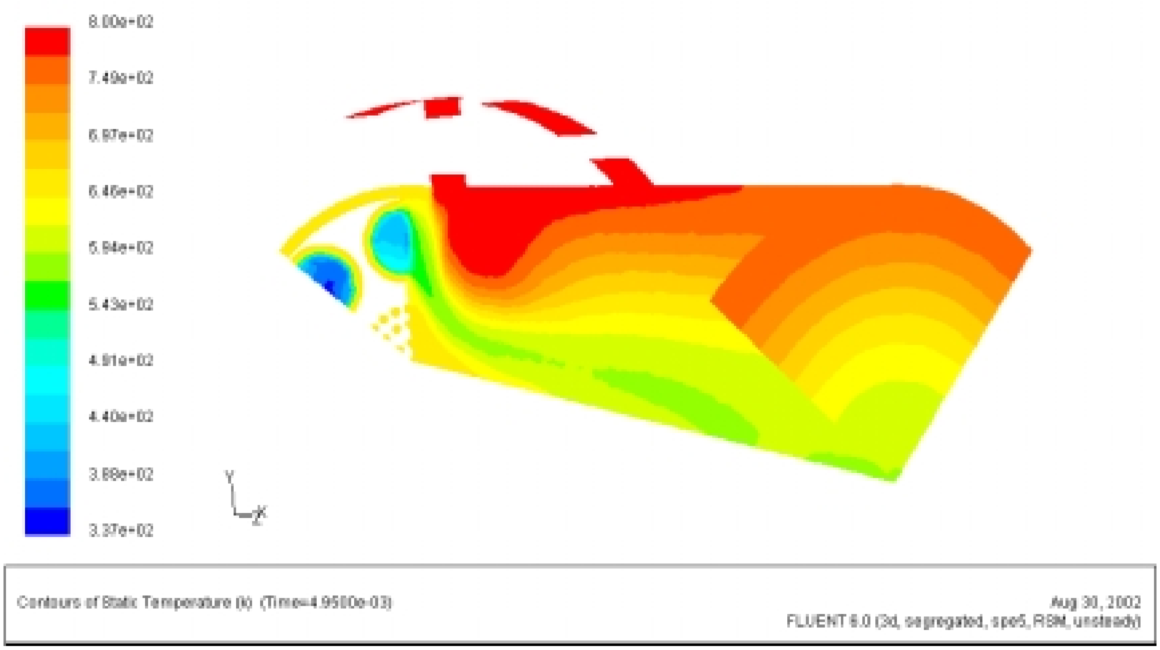

Figure 45: Temperature field after 5ms.

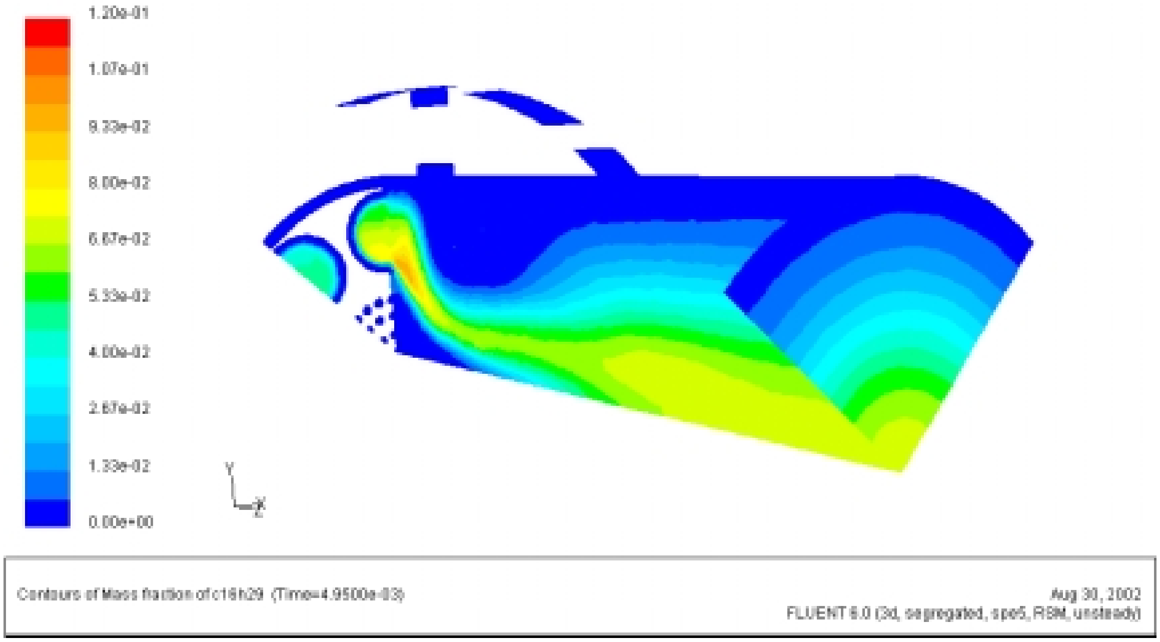

Figure 46: Fuel vapor mass fraction

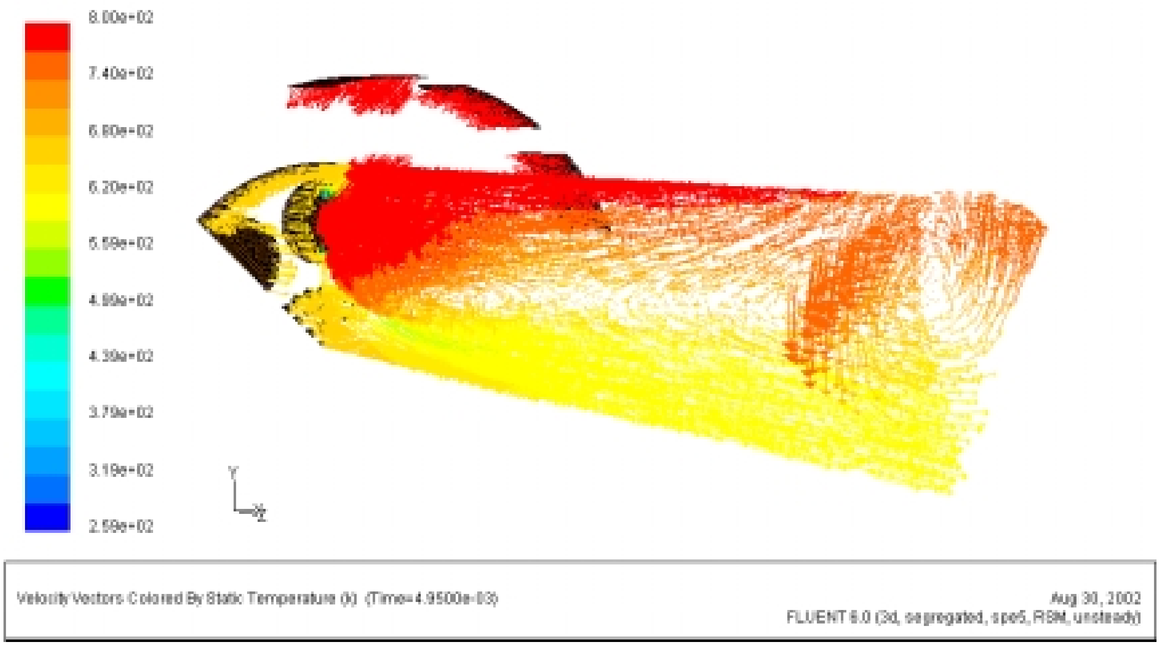

Figure 47: Velocity vectors colored by temperature

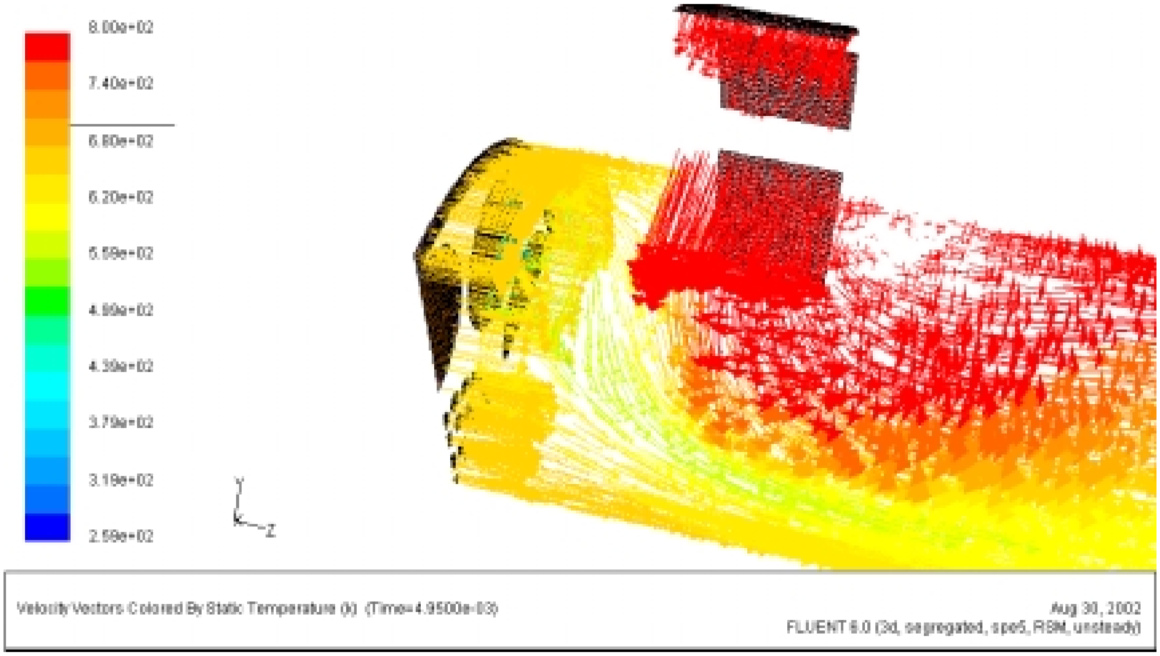

Figure 48: Alternative view of Figure 47

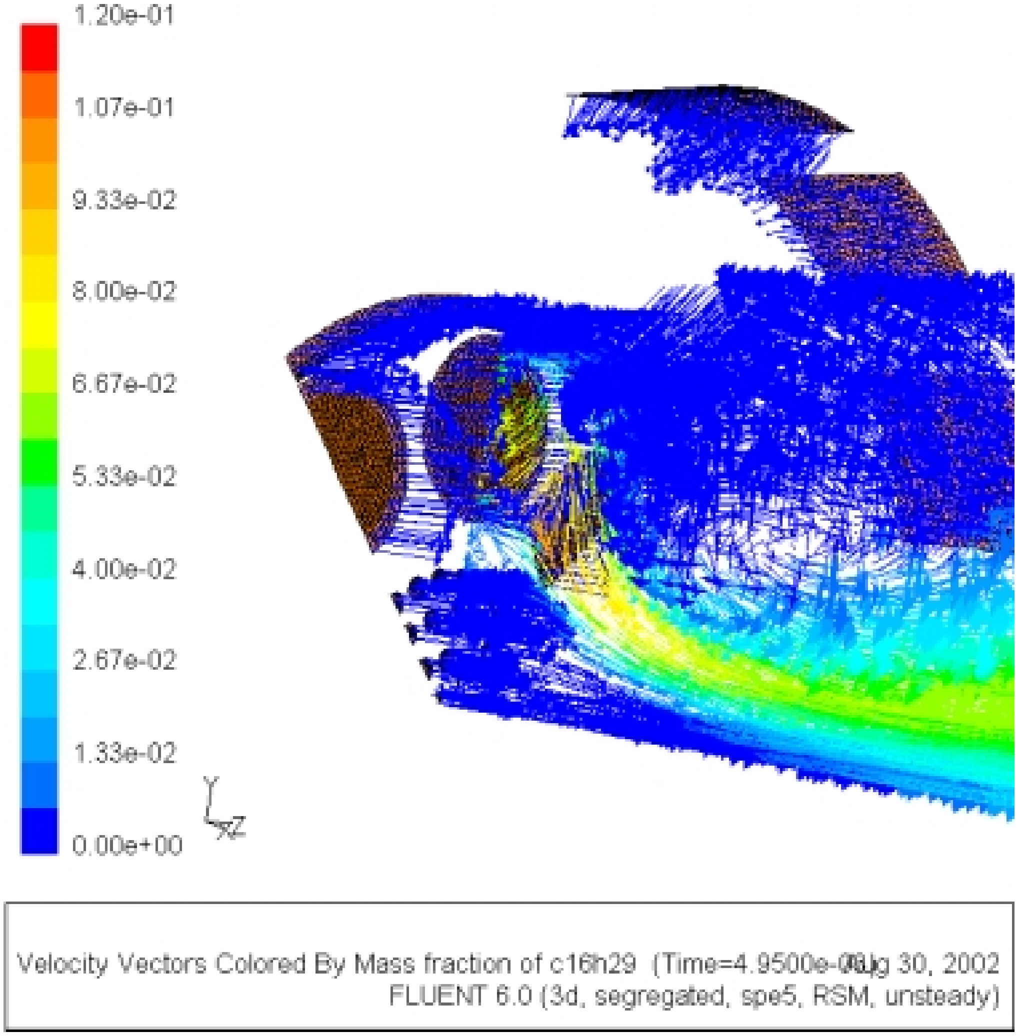

Figure 49: Velocity vectors colored by fuel vapor mass fraction

CONCLUSIONS AND RECOMMENDATIONS

The present research has extended the operation of the laboratory (1-2 atm) SPP into the range of short residence times and high temperatures. Residence times of 4-6 ms were run in the SPP, with the 1st stage temperature pushed into the 400-450 degrees C range, and the 2nd stage temperature pushed into the 550-600 degrees C range. When coupled to the 16 cc JSR, the SPP-JSR system provided NOx emissions as low as 6 ppmv (15% O_2 dry) for No. 2 diesel fuel burning at 1790 K.

These measurements demonstrate the ability of the SPP to operate at the short residence times and high air temperatures of gas turbine engines, and to provide the very low NOx emissions expected on LPP gas turbine engines.

The laser Rayleigh scattering measurements provide considerable insight on the mixedness of the SPP outlet stream, and on those SPP operating conditions that curtail the emission of droplets from the SPP and promote good mixedness of diesel-air mixture. Temperatures of 400-500 degrees C within the SPP appear to best for accomplishing optimal mixedness in the SPP outlet stream.

As future research, it is strongly recommended that a laboratory SPP be built and tested for high-pressure operation. Experience should be gained with the laboratory SPP operated at high pressure, short residence time, and high temperature, with the LRS diagnostics applied to study the goodness of vaporization and mixing obtained at high pressure.

The Energy and Environmental Combustion Laboratory of the University of Washington, with internal financial resources, has been building a high-pressure facility for the testing of laboratory-scale injectors and combustors. The air compressor, providing 800 #/hr of air at 25 atm, has been installed, and the air heaters, providing air at 550 degrees C, and the high-pressure vessel for housing the injector and combustor systems, are scheduled for installation in 2003.

With respect to the industrial scale SPP, the present research has led to the design and fabrication the SPP (by Parker Hannifin Corporation), and to the development of a setup (at Solar Turbines, Inc.) for the high-pressure testing of the industrial SPP. The high-pressure testing of the industrial SPP is scheduled for 2003 – after the termination of the present contract (AGTSR Subcontract 00-01-SR087).

CFD modeling has been applied to both the laboratory and industrial SPPs. This modeling provides insight on the flow, thermal, and fuel partners within the SPPs, and indicates about a ±10% spatial variation in the diesel vapor mass fraction in the outlet stream of the laboratory SPP. Particle (droplet) tracking indicates those SPP operating conditions that promote complete vaporization within the SPP. CFD modeling of the industrial SPP has helped to identify the flow, temperature, and fuel partners that might be expected during the high-pressure testing of the industrial SPP.

Once the high-pressure testing of the industrial SPP has been conducted and the results are analyzed, it will be possible to provide conclusions and recommendations regarding that work.

Acknowledges and Contributions

Several organizations and individuals have made this project possible and have contributed to its accomplishment. These organizations and individuals are thanked for their interests in and efforts on the project.

Primary funding for the project was provided by the Advanced Gas Turbine Systems Research group of the U.S. Department of Energy, through AGTSR Subaward No. 00-01-SR087.

The Gas Turbine Fuel System Division of the Parker Hannifin Corporation contributed through providing the design and fabrication of the industrial SPP. Additionally, PHC provided the original CFD grid of the industrial SPP.

Solar Turbines, Inc. is contributing through providing a site and personnel for the high-pressure testing of the industrial SPP.

Several individuals have provided material for this report:

- Material for the following sections of the report was drawn from the MSME Thesis of Mr. Ryan Edmonds:
    - Introduction
    - Laboratory SPP Modified for this Study – Experimental Setup
    - Testing the Laboratory SPP, Firing 16 cc Jet-Stirred Reactor

  Mr. Edmonds is now a Combustion Engineer with Ramgen Power Systems, Inc.

- Material for the following sections was provided by Mr. Andrew Campbell Lee:
    - Testing the Laboratory SPP, Firing 64 cc Jet-stirred Reactor
    - Testing the Laboratory SPP, with the Outlet Stream Examined by Laser Rayleigh Scattering

  Mr. Campbell is a Graduate Research Assistant in the MSME/PhD program of the Department of Mechanical, University of Washington.

- Material for the following sections was provided by Mr. Igor Novosselov:
    - CFD Modeling of the Laboratory SPP
    - CFD Modeling of the Industrial SPP

  Mr. Novosselov is a Pre-Doctoral Research Associate in the PhD program of the Department of Mechanical, University of Washington

- Dr. Stephen de Bruyn Kops, now Assistant Professor at the University of Massachusetts, Amherst, provided the formative CFD modeling on the laboratory SPP.

- Dr. Adel Mansour of the Gas Turbine Fuel System Division of Parker Hannifin Corporation provided the material for the section on the Industrial SPP.

- Dr. Kenneth O. Smith and Dr. John C. Y. Lee of Solar Turbines, Inc. provided material for the section on the Developing the Test Setup for the Industrial SPP.

References

Abraham, J. Williams, F.A. and Bracco, F.V. (1985), "A Discussion of Turbulent Flame Structure in Premixed Charges," SAE paper 850345, in Engine Combustion Analysis: New Approaches, P-156, pp. 27-43

Aigner, M., Engelbrecht, E.G., Eroglu, A., Hellat, J., Syed, K. (1999), "Development of an Oil Injection System Optimised to the ABB Double Cone Burner," ASME Paper No. 99-GT-218, ASME, New York.

Campbell, Jr., J.S. and Malte, P.C. (2002), "Integrating the Staged Prevaporizer-Premixer into Low-NOx Dual-Fuel Combustion," report, Department of Mechanical Engineering, University of Washington, Seattle, WA.

Campbell, Jr., J.S., Malte, P.C., de Bruyn Kops, S., Novosselov, I., Lee, J.C.Y., Benjamin, M.A. (2002), "Integrating the Staged Prevaporizer-Premixer into Gas Turbine Cycles," ASME Paper No. GT-2002-30081, ASME, New York.

Dibble, R. W. and Hollenbach, R. E. (1981), "Laser Rayleigh Thermometry in Turbulent Flames," *Proceedings of 18th Symposium (International) on Combustion*, pp. 1489-1499, The Combustion Institute, Pittsburgh, PA.

Edmonds, Ryan (2002), "Prevaporized Premixed Combustion at Short Residence Times," Masters of Science Thesis, University of Washington, Seattle, WA.

Espey, C. and Dec, J. (1997), "Planar Laser Rayleigh Scattering for Quantitative Vapor-Fuel Imaging in a Diesel Jet," *Combustion and Flame*, Vol. 109, pp. 65 – 86.

Gardiner, W. C., Hidaka, Y., and Tanzawa, T.(1981), "Refractivity of Combustion Gases," *Combustion and Flame*, Vol. 40, pp. 213 – 219.

Göttgens, J., Mauss, F. and Peters, N. (1992), "Analytical Approximations of Burning Velocities and Flame Thicknesses of Lean Hydrogen, Methane, Ethylene, Ethane, Acetylene and Propane Flames," *Twenty-Fourth Symposium (International) on Combustion,* pp. 129-135, The Combustion Institute, Pittsburgh, PA.

Laurendeau, N. M. (1991), "Temperature Measurements by Light Scattering Methods," *Combustion Measurements*. Edited by N. Chigier. Hemisphere Publishing Corp., pp. 95 – 142.

Lee, J.C.Y. (2000), "Reduction of NO_x Emission for Lean Prevaporized-Premixed Combustors," Ph.D. Dissertation, University of Washington, Seattle, WA.

Lee, J.C.Y. and Malte, P.C. (2001), "Staged Prevaporizer-Premixer," U.S. Patent No. 6,174,160B1, Jan. 16, 2001.

Lee, J.C.Y., Malte, P.C., and Benjamin, M.A. (2001), "Low NO_x Combustion for Liquid Fuels: Atmospheric Pressure Experiments using a Staged Prevaporizer-Premixer," ASME Paper No. 2001-GT-0081, ASME, New York.

Lefebvre, A.H. (1989), *Atomization and Sprays*, Taylor & Francis, Bristol, PA.

Lefebvre, A.H. (1999), *Gas Turbine Combustion*, 2nd Ed., Taylor & Francis, Philadelphia, PA.

Rutar, T., Horning, D.C., Lee, J.C.Y. and Malte, P.C. (1998), "NO_x Dependency on Residence Time and Inlet Temperature for Lean-Premixed Combustion in Jet-Stirred Reactors," ASME Paper No. 98-GT-433, ASME, New York.

Schorr, M.M., Chalfin, J.(1999), "Gas Turbine NO_x Emissions Approaching Zero-Is it Worth the Price?", GER 4172, GE Power Generation, Schenectady, New York.

Spadaccini, L.J. and TeVelde, J.A. (1982) , "Autoignition Characteristics of Aircraft-Type Fuels," *Combustion and Flame*, Vol. 46, pp. 283 – 300.

Turns, S. T. (2000), *An Introduction to Combustion: Concepts and Applications*, 2nd Ed. McGraw-Hill, New York.

Yee, D. (1982), "Experimental Study of Turbulent Mixing in Nonburning and Burning Hydrogen-Air Coaxial Jets," Ph. D. Dissertation. Washington State University, Pullman, WA.